FACULTY OF SCIENCE AND TECHNOLOGY

MASTER'S THESIS

Study programme/specialisation: Master of Science in Petroleum Engineering – Reservoir Engineering	Spring semester, 2017 Open
Author: Sebastian White	…… (signature of author)
Programme coordinator: Aksel Hiorth	
Title of master's thesis: Streaming Potential in Porous Media – Single and Two-Phase	
Credits (ECTS): 30	
Keywords: Streaming potential Zeta potential Electrokinetic phenomena Electrokinetic coupling Multi-phase flow	Number of pages: 80 Stavanger, June 15/2017 date/year

Title page for Master's Thesis
Faculty of Science and Technology

Abstract

The streaming potential method is a promising method to measure how surface potential change when different fluids are injected into a rock. The understanding of how and why the surface potential changes can give important information about the transport of oil and water, and which brines to use in a water flood to improve the oil recovery. The interpretation of streaming potential measurements are straightforward for single-phase flow in homogenous, porous rocks. In the presence of oil, the interpretation is much more complicated. Recent experimental studies claim that a change in the streaming potential is independent of saturation, and only indicates wettability change, while simple analytical models predict a correlation between fluid saturations and streaming potential. In this thesis, appropriate theory for the interpretation of streaming potential measurements are first presented. Further, the well-known Helmholtz-Smoluchowski equation for single phase streaming potential, in addition to simple analytical models of two-phase streaming potential developed by Sherwood (2007) are derived from first principles. The two-phase models are analysed and discussed in order to investigate the effects of an oil phase on the measured streaming potential. The results of the analysis indicate that the total streaming potential in a water-oil system most likely represents a combination of effects arising from wettability and movement of charged- and uncharged oil particles. The total effect is highly dependent on the interface properties at the particle surface.

Acknowledgements

I would like to thank my supervisor Professor Aksel Hiorth both for presenting me with this interesting and challenging topic, and for his guidance throughout the last semester. His scientific insight is inspiring and his feedback has been central for the quality of this thesis.

In addition, I would like to thank Associate Professor Anders Nermoen, Senior Research Scientist at IRIS Nils Harald Giske and fellow MSc student Bendik Horvei for valuable discussions during meetings this last semester.

Finally, I would like to thank my fellow MSc students for fruitful discussions, and my family and close friends for all their help and understanding.

Table of contents

Abstract I
Acknowledgements III
Table of contents V
List of Figures VII
List of Tables IX
Nomenclature XI
Chapter 1. Introduction 1
1.1. Background and Objectives 1
1.2. Thesis Outline 2
Chapter 2. Wettability 3
2.1. Wettability of Mineral Surfaces 3
2.1.1. Acting Forces 4
2.1.2. Mathematical Description 6
2.1.3. Measuring 7
2.2. Wettability of Porous Media 8
2.2.1. Wettability Index for Porous Media 8
2.2.2. Recent Developments of Wettability Measurements 9
Chapter 3. Electrochemistry 12
3.1. Surface Charge 12
3.2. Poisson's Equation 14
3.3. Electrical Double Layer 17
3.3.1. Electrical Double Layer for Flat Surfaces 18
3.4. Zeta Potential 22
3.5. Electrokinetic Phenomena 24
Chapter 4. Fluid Flow 26
4.1. Navier-Stokes Equation 26
4.2. Poiseuille's Equation 31
Chapter 5. Streaming Potential 34
5.1. Single Phase Streaming Potential 34
5.1.1. Helmholtz-Smoluchowski's Equation for Single Phase Streaming Potential 36
5.2. Two-Phase Streaming Potential 40
5.2.1. Single Spherical Droplet in a Capillary 41

5.2.2. A Line of Non-Interacting Spherical Particles 46
Chapter 6. Analysis of the Two-Phase Models 48
6.1. Single Spherical Droplet Model 48
6.2. A Line of Non-Interacting Spherical Particles 54
Chapter 7. Discussion 58
7.1. Results from Model Calculations and Experimental Data 58
7.2. The Effect of Particle (Drop) Boundary Condition 59
Chapter 8. Conclusion 61
8.1. Concluding Remarks 61
8.2. Suggestions for Future Work 61
References 62

List of Figures

Figure 2.1 Drop of oil on a preferentially water-wet surface A, neutral wet surface B, and preferentially oil-wet surface C, surrounded by water. The contact angles vary from respectively $\varphi < 90°$, $\varphi = 90$, and $\varphi > 90°$. Modified from Ziauddin et al. (2007). 3
Figure 2.2 Structure and Partial Charges of the Water Molecule. 4
Figure 2.3 Partial Wetting of Water on a Solid Surface. Modified from Ziauddin et al. (2007). 6
Figure 2.4 Partial Wetting of Oil on a Solid Surface. Modified from Ziauddin et al. (2007). 6
Figure 2.5 Zeta potential as a function of water saturation aged with oil in (a) 2M NaCl and (b) formation brine. Empty circle denotes aging of oil-only, empty squares denote aged samples in presence of water, filled square denotes non-aged sample and diamond represents single phase water sample. From (Al-Mahrouqi, 2016), p. 121. 10
Figure 2.6 Zeta potential as a function of water wetting index saturated with 2M NaCl (NaB) or formation brine (FMB1) and residual oil saturation. Again, empty circle denotes aging of oil-only, empty squares denote aged samples in presence of water, filled square denotes non-aged sample and diamond represents single phase water sample. From (Al-Mahrouqi, 2016), p.125. 11
Figure 3.1 A point charge with corresponding lines of force and equipotential surfaces. 14
Figure 3.2 Simple illustration of the electrical double layer at static conditions, with negatively charged quartz surface. Ideally, the two regions of the EDL balance the surface charge on the solid such that the total electric charge remains neutral. 18
Figure 3.3 Illustration of zeta potential with respect to the shear plane and the electrical double layer for a quartz surface. The Stern layer can consist of different types of cations (marked green and blue). 23
Figure 4.1 Illustration of the velocity profile for laminar flow of a Newtonian fluid. A fluid element is indicated, this is further described in Figure 4.2. 27
Figure 4.2 Left: Illustration of arbitrary fluid elements with associated velocities. Right: Definition of the dimensions of an arbitrary fluid element. 28
Figure 4.3 Three-dimensional fluid element with pressure difference $\Delta pz = p1 - p2$ indicated. 29
Figure 4.4 Capillary tube with length and radius indicated in addition to pressure difference, flow direction and direction of the pressure force and viscous force. 31
Figure 4.5 Left: The velocity gradient as expressed by equation (4.2.5). Right: The corresponding velocity profile in a tube. 32
Figure 5.1 Illustration of streaming potential. The streaming current Is forms in the EDL in the direction of fluid flow. The conduction current Ic moves in the opposite direction through the bulk fluid. Total measured electric potential is the streaming potential. 35
Figure 5.2 Fluid flow in a capillary tube. For simplicity reasons, x denotes the distance from the capillary wall. Modified from Hunter (1981). 37
Figure 5.3 Illustration of the spherical particle of radius Rp in a capillary of radius $Rc = Rp + h0$. Lengths are not to scale. Modified from Sherwood (2007). 41
Figure 6.1 Definition of the local water saturation $Sw'Rc, Rp$. Lengths are not to scale. 51
Figure 6.2 Normalised streaming potential vs. local water saturation for different capillary radii. 52

Figure 6.3 Normalised streaming potential vs. $(1 - Rp/Rc)$, where Rp/Rc represents the droplet size compared to capillary radius. 53
Figure 6.4 Definition of water saturation for a capillary filled with a line of spherical particles $Sw'Rc, Rp, Lc, N$. 55
Figure 6.5 Normalised streaming potential vs. water saturation for small and large droplets. In addition, the single phase water line is indicated. 56
Figure 6.6 Normalised two-phase streaming potential vs. water saturation for different values of zeta potential on the particle (ζp). 57
Figure 7.1 Illustration of the surface of a charged particle of oil dispersed in water with corresponding fluid velocity profile. The small spheres on the surface represent polar head-groups with a non-polar tail. The fluid moves in z-direction with velocity vz. The polar head-groups decrease the fluid velocity to zero close to the particle surface. 60

List of Tables

Table 1 Limiting values for lubrication theory. 50
Table 2 Values used for calculation of two-phase streaming potential (spherical model)..... 51

Nomenclature

Symbol/Abbreviation	Description	SI Unit
a	Acceleration	m/s^2
A	Area	m^2
c_0	Brine salinity	mol/l
C_{SP}	Streaming potential coupling coefficient	V/Pa
D	Volumetric mass density	kg/m^3
e	Electric charge of an electron	C
E	Electric field strength	V/m
E_{bubble}	Two-phase streaming potential for uncharged spherical bubble	V
E_c	Streaming potential due to zeta-potential on the capillary wall	V
E_p	Streaming potential due to zeta-potential on the particle surface	V
E_s	Streaming potential	V
E_{line}	Two-phase streaming potential for a line of rigid spherical particles	V
$E_{line,norm}$	Two-phase streaming potential for a line of rigid spherical particles, normalised	V
E_{sp}	Two-phase streaming potential for rigid spherical particle	V

$E_{sp,norm}$	Two-phase streaming potential for rigid spherical particle, normalised	V
F	Force	N
F_e	Electromagnetic force	N
F_p	Pressure force	N
F_v	Viscous force	N
G	Pressure gradient	Pa/m
h	Height	m
h_0	Minimum particle-capillary gap width	m
I_s	Streaming current	A
I_c	Conduction current	A
k	Permeability	m^2
k_B	Boltzmann constant	J/K
l	Cylindrical length of a long drop	m
L	Length	m
M	Viscosity ratio	-
n	Porosity	-
n_i	Concentration of ions of type i	mol/L
n_i^0	Concentration of ions of type i in the bulk solution	-
p	Pressure	Pa
q	Volumetric flow rate	$m^3/_s$
Q	Electric charge	C
r	Radius of investigation	m

R	Radius	m
R_c	Radius of capillary	m
R_p	Radius of particle	m
S_w	Water saturation	-
S'_w	Local water saturation	-
t	Time	s
T	Absolute temperature	K
u	Droplet velocity	m/s
v	Average fluid velocity	m/s
v_z	Linear velocity in z-direction	m/s
V	Volume	m^3
V_c	Volume of capillary tube	m^3
V_0	Volume of oil phase	m^3
V_w	Volume of water phase	m^3
x	Distance from capillary wall	m
z_i	Valence of ion i	$-$
γ	Interfacial tension	Pa
δ	Coefficient of proportionality	-
Δ	Difference operator	-
∇	Del operator	-
ε	Permittivity	F/m
ε_0	Permittivity in vacuo	F/m
ζ	Zeta potential	V

ζ_c	Zeta potential on capillary wall	V
ζ_p	Zeta potential on particle	V
η	Dynamic viscosity	$Pa \cdot s$
η_d	Dynamic viscosity of drop	$Pa \cdot s$
κ	Debye-Hückel parameter	m^{-1}
κ^{-1}	Debye length	m
λ_0	Bulk conductivity	S/m
λ_s	Surface conductivity	S/m
μ	Chemical potential	J
ρ	Electric charge density	C/m^3
σ	Shear stress	Pa
τ	Tortuosity	-
φ	Angle	° $(Degrees)$
Ψ	Electric potential field	V

Chapter 1. Introduction

1.1. Background and Objectives

Streaming potential is an electrical potential generated by fluids moving through a capillary or porous medium. The streaming potential method is a promising method to measure how surface potential change when different fluids are injected into a rock. This method has been known for some time, but only recently been applied to porous rocks at conditions relevant for petroleum production, which means that there are still significant uncertainties related to both measurements and interpretation of results. The understanding of how and why the surface potential changes can give important information about the transport of oil and water, and which brines to use in a water flood to improve the oil recovery. The interpretation of streaming potential experiments are straightforward for single-phase flow in homogenous, porous rocks. In the presence of oil, the interpretation is much more complicated.

Recent experimental results show a correlation between measured streaming potential and the wetting state of reservoir rocks, independent of saturations, while simple analytical models predict a correlation between fluid saturations and streaming potential. This requires further research. This thesis will present derivations of two simple analytical models from first principles, and address the relationship between the model predictions and experimental results in order to achieve an understanding of how the presence of an oil phase affects the streaming potential.

1.2. Thesis Outline

The thesis is divided into eight chapters. Chapter 2 aims to build a theoretic foundation for our understanding of wettability in order to discuss how streaming potential can be related to wettability later in the thesis.

Chapter 3 presents theoretical aspects of electrochemistry, which serves to explain the origin of electrokinetic phenomena, including streaming potential. This chapter also includes the derivation of Poisson's equation which is used later in the derivation of Helmholtz-Smoluchowski's equation for streaming potential.

Electrokinetic phenomena combine the effects of electrochemistry and fluid flow. Chapter 4 concerns fluid flow and includes the derivation of Poiseuille's equation from first principles.

In Chapter 5, the theory of streaming potential is presented both for single phase and two-phase flow. This chapter includes the derivations of Helmholtz-Smoluchowski's equation and of the two-phase streaming potential models we will analyse further.

The analysis of the two-phase models are presented in Chapter 6 and are further discussed in Chapter 7. Finally, concluding remarks and suggestions for future work are presented in Chapter 8.

Chapter 2. Wettability

A basic understanding of wettability is important for the further discussions regarding streaming potential measurement as an indicator of rock wettability. Wettability is one of the most important parameters in order to determine how fluids are transported through a porous rock. The wetting of the pore surface determine which fluid it is in contact with. Wetting affects hydrocarbon reservoir behaviour and recovery (Ziauddin et al., 2007). Different methods have been developed in an attempt to estimate the exact wetting preference of reservoir rocks, as well as to alter the rock wettability (Ziauddin et al., 2007). The wetting state of a mineral surface can usually be determined by contact angle measurements, whereas the wetting state of a porous rock is usually related to the production of oil and water.

2.1. Wettability of Mineral Surfaces

By placing a drop on a surface the fluid will spread out on the surface and displace the initial liquid or gas to different degrees, depending on the wettability. The fluid spreads out until the solid-fluid angle reaches a specific value known as the *contact angle*. This angle is defined through the densest fluid in the system, and it essentially determines the wettability of the flat surface (Ziauddin et al., 2007).

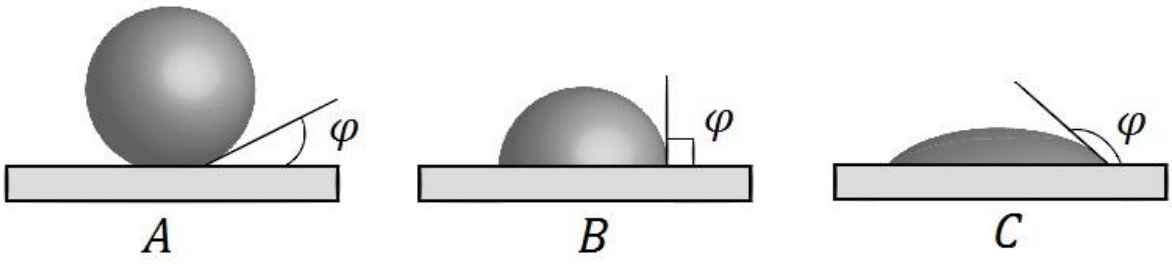

Figure 2.1 Drop of oil on a preferentially water-wet surface A, neutral wet surface B, and preferentially oil-wet surface C, surrounded by water. The contact angles vary from respectively $\varphi < 90°$, $\varphi = 90$, *and* $\varphi > 90°$. *Modified from Ziauddin et al. (2007).*

The contact angle varies between zero and 180 degrees. In an oil-water system, the surface is said to be water-wet if the contact angle is less than 90°, and consequently oil-wet if it is larger than 90° (Berg, 1993). In the special case when the angle is exactly 90°, the surface

is referred to as neutral-wet, not to be confused with mixed wetting which will be described later (Berg, 1993; Ziauddin et al., 2007).

2.1.1. Acting Forces

There are two main forces that control wetting and the liquid-solid contact angle; cohesion and adhesion. They are the forces that determine how well liquid molecules 'stick' to themselves or to other substances respectively.

The strong cohesive properties of water is mainly caused by the electric forces in the dipolar water molecule. The inclination between the two hydrogen atoms and the oxygen atom in the water molecule (Figure 2.2) causes the side with the hydrogen atoms to have a slight positive charge, and the side with the oxygen atom to have a slight negative charge. Consequently, the molecules will align and be attracted to each other by electrical forces, which causes cohesion (Campbell & Reece, 2002; Young, 1805).

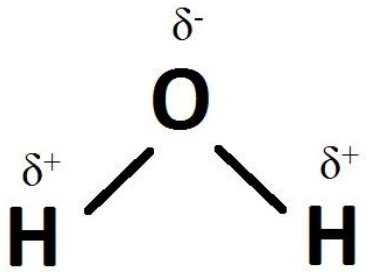

Figure 2.2 Structure and Partial Charges of the Water Molecule.

Even though many crude oils contain polar components, which can give the oil some polar properties (Bastow, van Aarssen, & Lang, 2007), oil molecules themselves are non-polar. In the case of non-polar oil, no electrical forces act to stick the oil to itself. Instead, oil forms weak cohesion due to *Van der Waals* forces. These forces induce polarity in non-polar molecules. Van der Waals forces arise from statistical quantum mechanics and are relatively weak forces between molecules.

Van der Waals forces can be divided into three subtypes: Keesom-, Debye- and London forces. Keesom forces are electrostatic interactions between permanent dipoles. Forces between one permanent dipole and a corresponding induced pole are called Debye forces. London forces arise from instantaneous polarization in molecules (Dzyaloshinskii, Lifshitz, & Pitaevskii, 1961; Tadmor, 2001).

Adhesion is the ability of a substance or surface to be attracted to other, dissimilar substances. The actual mechanisms causing adhesion are not fully understood, nor explained by a single theory. Five main mechanisms have been put forward to describe adhesion:

- Dispersive
- Mechanical
- Chemical
- Electrostatic
- Diffusive

Dispersive adhesion, also called physisorption, is widely recognized as the most important mechanism of adhesion. Dispersive adhesion is the attraction between two substances due to van der Waals forces.

Mechanical adhesion occurs when two adhesive materials form a mechanical bond by interlocking. Large scale examples of this are the hooks and loops in Velcro.

Chemical adhesion takes place when two substances form a chemical compound bounded by covalent or ionic bonds.

Electrostatic adhesion is when materials form an electric potential at the joint caused by difference in electrical charge. This form of adhesion is possible for electrically conductive materials. The two substances are then attracted by the electrostatic force.

Diffusive adhesion refers to the net transport of atoms from one material to the other caused by random thermally activated movement. Leaking of helium through the walls of a balloon is an example of atomic diffusion. This can happen on a small scale to make two materials stick together as atoms of each material blend into each other.

The stronger of the cohesive/adhesive forces for each solid-fluid system determine the wetting state. In a petroleum reservoir containing several different fluids, the fluid with the most adhesive properties (with respect to the reservoir rock) is referred to as the wetting phase (Israelachvili, 1985; Kendall, 1994; London, 1937).

2.1.2. Mathematical Description

The most common equation used to describe the wetting properties of a flat rigid surface, or to predict the contact angle of a system is Young's equation. It states the mathematical relation between the interfacial tension γ (of the liquid-gas, solid-gas and solid-liquid respectively) and the contact angle φ:

$$\gamma_{LG} \cdot cos\varphi = \gamma_{SG} - \gamma_{SL}, \tag{2.1.1}$$

assuming an *ideal surface*. Figure 2.3 below illustrates partial wetting of water on a solid surface (Butt, Graf, & Kappl, 2006).

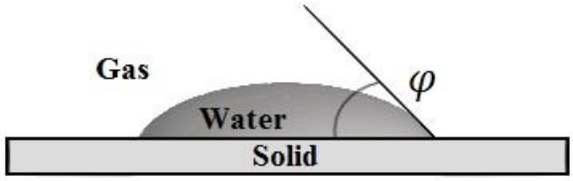

Figure 2.3 Partial Wetting of Water on a Solid Surface. Modified from Ziauddin et al. (2007).

For contact angles between 0 and $90°$, $cos\varphi$ is positive (and interfacial tensions are always positive), thus γ_{SG} must be larger than γ_{SL}. In this case there is partial wetting of the liquid phase. Similarly, when gas is the wetting phase, $cos\varphi$ is negative, which means that the solid-liquid interfacial tension is larger than the solid-gas interfacial tension. Thus, the wetting preference of the solid can be computed by determining the surface energy of each phase in the system.

Young's equation also applies when the surrounding fluid is a liquid, given that the two liquids are immiscible. In an oil-water-solid case as illustrated in Figure 2.4, the interpretation of equation *(2.1.1)* is similar as for the gas-water-solid case above.

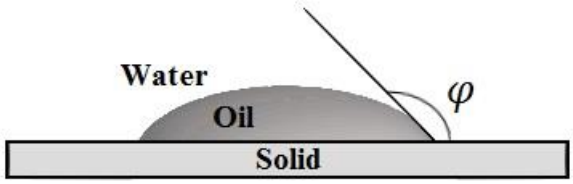

Figure 2.4 Partial Wetting of Oil on a Solid Surface. Modified from Ziauddin et al. (2007).

2.1.3. Measuring

One way of determining the wetting preference of a flat mineral surface is to measure the contact angle between the solid and the liquid. The most common way to do this is to observe a sessile drop (liquid droplet on a solid) with a telescope or microscope. The contact angle can then be measured directly with a goniometer, or the shape of the droplet can be matched by a computer using the Young-Laplace equation. The contact angle can also be calculated by measuring the height h and radius r of the droplet using the following equation, assuming that the droplet has a circular cross-section (Butt et al., 2006):

$$\tan\left(\frac{\varphi}{2}\right) = \frac{h}{r}. \qquad (2.1.2)$$

2.2. Wettability of Porous Media

Porous media wettability describes which fluid preferentially adheres to the solid surface in a system consisting of a solid porous medium and two or more fluid phases. The different physical forces discussed in chapter 2.1.1 determine how a fluid either spreads out on the surface or coheres to itself. Wetting forces are very important in the petroleum industry as they influence reservoir behaviour and hydrocarbon recovery (e.g. (Austad, 2013; Morrow, 1990)).

The wetting state of reservoir rocks in petroleum systems is complex. Inhomogeneous wetting may be caused by differences in chemical composition or migration of fluids. Even though the whole reservoir was initially water-wet, the parts of the rock that have only been exposed to water may remain water-wet, while parts of the rock that has been exposed to oil may become oil-wet. Typically, the most abundant minerals in reservoir rocks are water-wet. (Berg, 1993; Ziauddin et al., 2007).

2.2.1. Wettability Index for Porous Media

Perhaps the most widely used method for wettability classification of a porous rock is a test first described by Amott (1959). Here, wettability is measured as a function of the displacement properties of the system. The test is divided into four parts; spontaneous displacement of water by oil, forced displacement of water by oil, spontaneous displacement of oil by water, and forced displacement of oil by water. The ratios of spontaneous displacement volumes to the total displacement volumes determines the wettability indices for water (I_w) and oil (I_o).

Another common method for measuring wettability is the USBM method, developed by the US Bureau of Mines. A core sample at irreducible water saturation is placed in a water-filled tube and put in a centrifuge. Eventually, the sample reaches residual oil saturation. Then, the sample is placed in an oil-filled tube for further measurements. The USBM wettability index is given by the area under the capillary-pressure curves for the sample (Ziauddin et al., 2007).

2.2.2. Recent Developments of Wettability Measurements

The challenge with the USBM and Amott wettability index is the fact that they assume that the rock wettability does not change during imbibition. However, in recent decades it has become more and more apparent that the injected brine can affect the wetting state of the rock (e.g. (Austad, 2013)). It is therefore extremely valuable to have some way of monitoring the wetting state in-situ during the imbibition process. It has been suggested in recent papers that there is a correlation between the measured streaming potential and two-phase wetting preference of reservoir rocks (Al-Mahrouqi, 2016; Jackson & Vinogradov, 2012; Rahbar et al., 2017). Streaming potential measurements can provide valuable information about the electrokinetic properties of a solid-liquid interface, which seemingly can be correlated with rock wettability, and more specifically, the Amott wetting-index (Al-Mahrouqi, 2016).

In Al-Mahrouqi's experiments, the Amott water index and the zeta potential (ζ) was interpreted for different water saturations of aged and non-aged core samples. Two different samples showed identical zeta potentials within experimental error for water-only and non-aged samples, indicating that the zeta potential is independent of saturation. For aged samples, the measured zeta potential decreased with decreasing water saturation (Figure 2.5). When compared to wettability, a linear regression was ascribed to each rock/brine/oil combination and expressed as

$$\zeta(I_w) = C \cdot \log(I_w) + \zeta_{Sw=1},$$

for

$$C = \frac{d\zeta}{d(\log(I_w))}.$$

The experimental results indicated that a decreasing water-wetness (I_w) consistently yields more negative zeta potential (Figure 2.6).

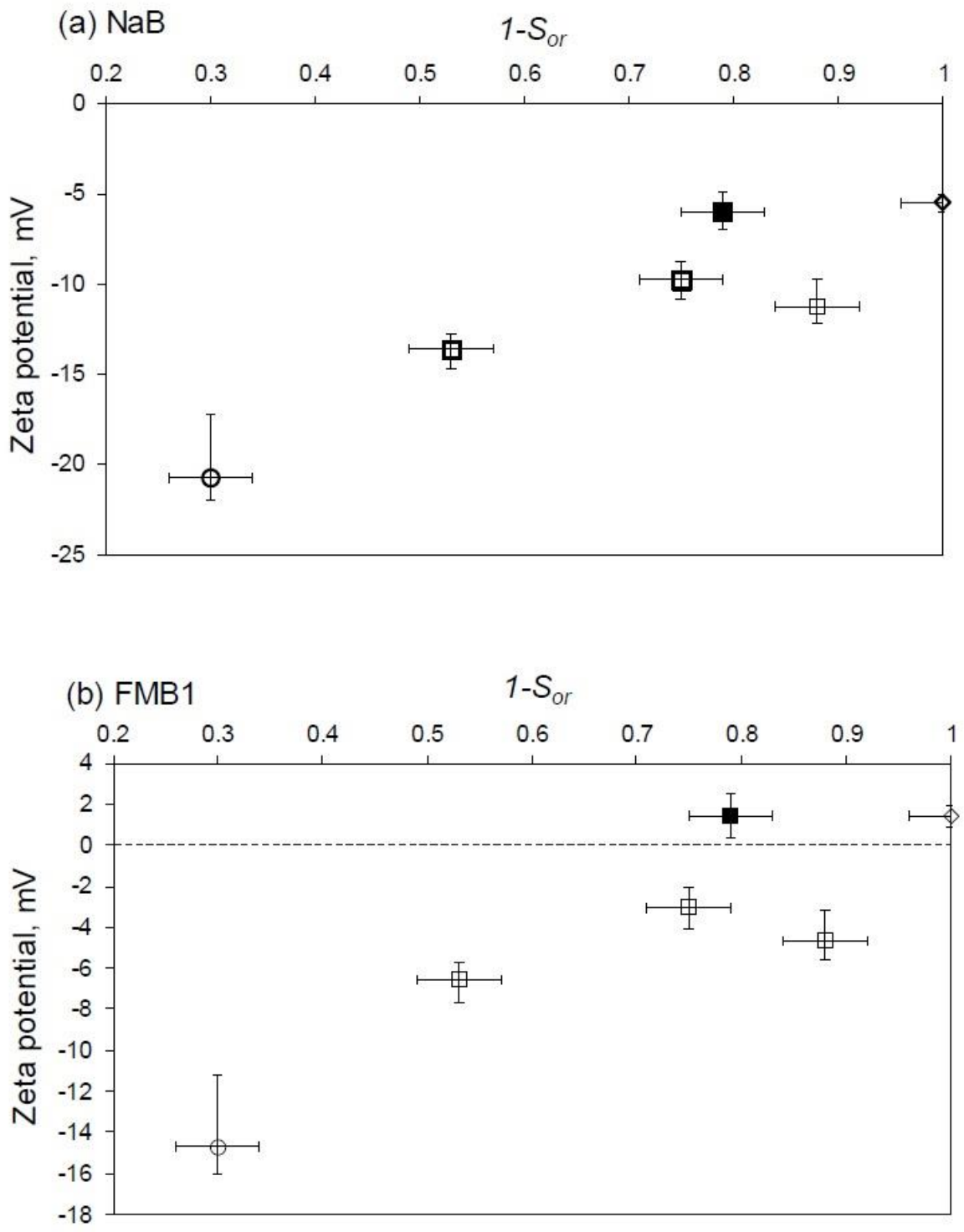

Figure 2.5 Zeta potential as a function of water saturation aged with oil in (a) 2M NaCl and (b) formation brine. Empty circle denotes aging of oil-only, empty squares denote aged samples in presence of water, filled square denotes non-aged sample and diamond represents single phase water sample. From (Al-Mahrouqi, 2016), p. 121.

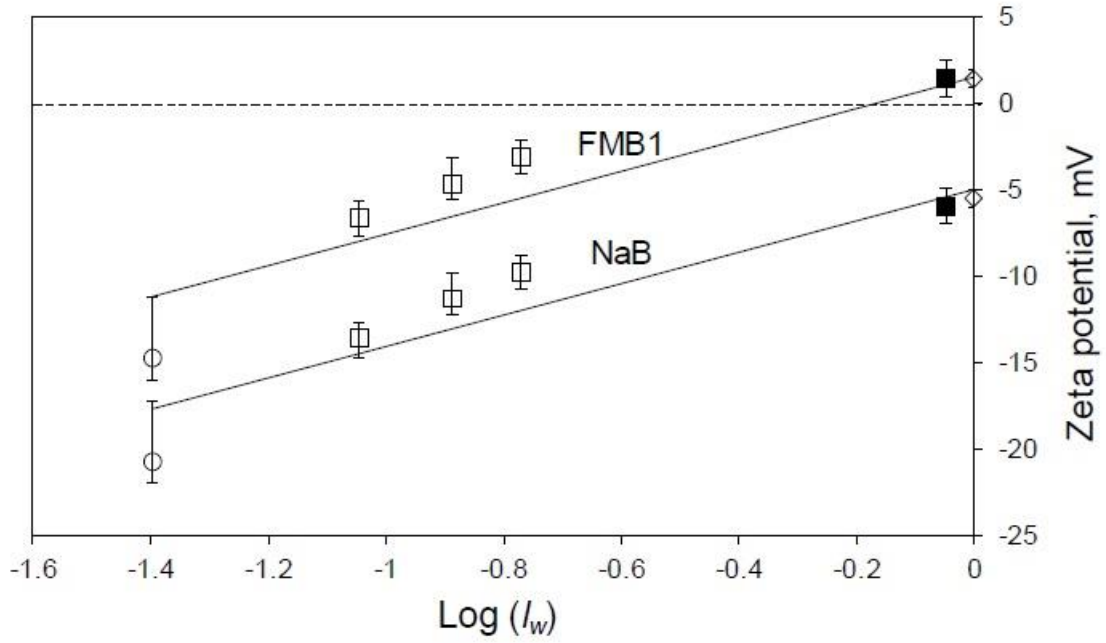

Figure 2.6 Zeta potential as a function of water wetting index saturated with 2M NaCl (NaB) or formation brine (FMB1) and residual oil saturation. Again, empty circle denotes aging of oil-only, empty squares denote aged samples in presence of water, filled square denotes non-aged sample and diamond represents single phase water sample. From (Al-Mahrouqi, 2016), p.125.

Chapter 3. Electrochemistry

This chapter will present theoretical aspects of electrochemistry, such as the development of surface charge, the electrical double layer, zeta potential, and electrokinetic phenomena, as presented by e.g. Hunter (1981) and Butt (2006). This is done to explain the origin of electrokinetic phenomena, including the streaming potential. In addition, mathematical descriptions such as Poisson's equation for description of electrostatic interactions at solid-liquid interfaces, and consequently a model for the electrical double layer at flat surfaces are presented and discussed. These equations will be used in further mathematical derivations, and in the physical interpretation of models for two-phase fluid flow.

3.1. Surface Charge

When a solid is immersed in a liquid, the solid surface acquires an electric charge. Simply put, this occurs because a very thin layer of the solid surface is dissolved in the liquid phase. The surface charge induces an electric field on the surface, which can affect many properties in the solid-fluid system (Butt et al., 2006).

The formation of surface charge can be caused by different mechanisms. One of the mechanisms at play is *dissociation*. This is a process where chemical compounds separate into smaller particles, which can release charged particles (e.g. H^+) in the fluid, leaving the surface with an electric charge. The relative concentration of dissolved H^+ and OH^- can determine the magnitude and sign of the surface charge. Thus, the surface charge is a function of solution pH (e.g. (Schindler & Stumm, 1987)). Another mechanism is when a molecule (e.g. a mineral in the solid) exchanges an atom with one that has a higher or lower number of ions than the original atom. An example of this is when the Si atom in SiO_2 (quartz) is replaced by an Al atom. Since Al has less electrons than Si, the quartz surface acquires a negative electric charge. A third way surface charge is formed is by partial charges of the solid. The partial charges occur because the neutral atoms in the solid are chemically bound together. The atoms align themselves in a certain way to form the chemical bond, which causes them to acquire a partial charge (i.e. slightly more positively/negatively charged on one side). The partial charges on the surface attracts ions from the fluid to form the surface charge (Atkins & De Paula, 2010; Hiemenz & Rajagopalan, 1997; Stumm, 1992).

The formation of surface charge also depends on the type of fluid in the system. Water has high relative permittivity (relative to permittivity of vacuum), also known as dielectric constant ε ($\varepsilon_w \approx 80$ at 20°C, $\varepsilon_w \approx 58$ at 90°C) (Malmberg & Maryott, 1956). Permittivity is a materials capacity to resist the electric field strength. The relative permittivity expresses how much the electric field between two point charges is decreased relative to vacuum. This means that water can more easily dissolve ions from a solid surface, than for example oil. Hydrocarbons have low relative permittivity ($\varepsilon_{HC} \approx 1.95 - 2.05$ at 20°C and $\varepsilon_{HC} \approx 1.85 - 2.00$ at 90°C for C8-C16) (Carey & Hayzen, 2001). Oil can thus not as easily dissolve ions from a solid surface. The result is less surface charge for a porous medium immersed in oil (Butt et al., 2006).

In a petroleum system, the mechanisms discussed applies to the porous reservoir rock to create an electrical surface charge of the formation. Petroleum reservoirs often have a large surface to volume ratio, which can make the effects of interfaces important. Typical reservoir rocks on the Norwegian continental shelf (NCS) are limestone and sandstone. Limestone consists of calcite ($CaCO_3$) which acquires a positive or negative surface charge in water, depending on the pH. Sandstone is mainly comprised of quartz (SiO_2) and often contains clay minerals, both of which becomes negatively charged when immersed in water.

3.2. Poisson's Equation

Poisson's equation describes electrostatic interactions at a charged interface between a solid and an ionic solution. It relates the electric potential generated at the interface to the electric charge density and permittivity of the solution. The equation will be used to further describe electrostatic- and electrokinetic effects at interfaces.

If we consider a point charge, the surrounding electrostatic potential is the same for all points on a sphere centred on the charge. All concentric spheres will represent an equipotential surface with decreasing potential as the spheres increase in size. Since the spheres are concentric, the lines of force from the point charge will be normal to the spheres. Furthermore, for a charge- or potential distribution, the equipotential surfaces will have a more complex shape (Hunter, 1981).

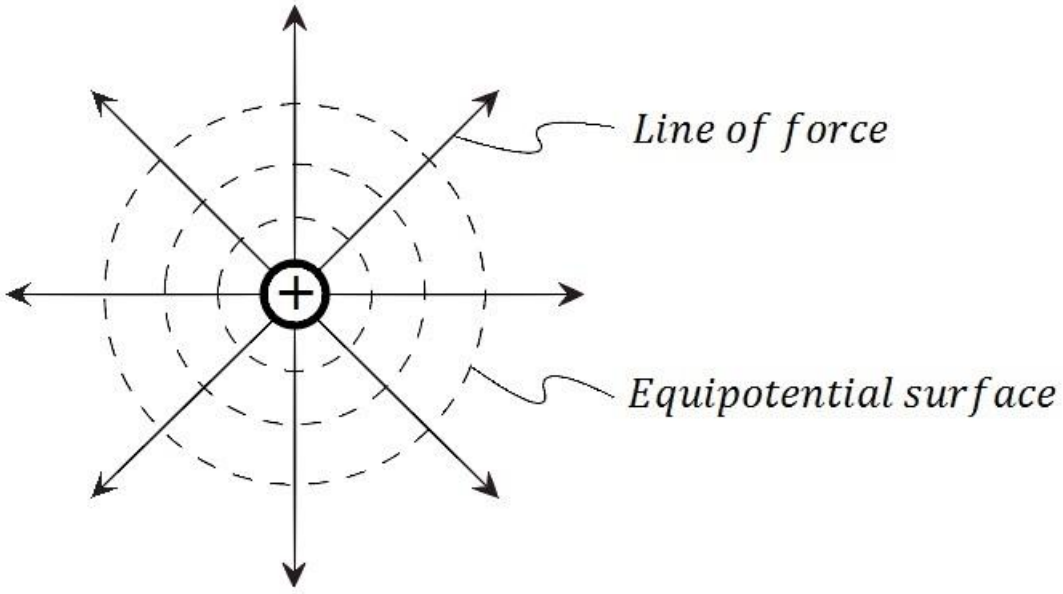

Figure 3.1 A point charge with corresponding lines of force and equipotential surfaces.

The gradient of the potential describes how the potential changes with respect to position, i.e. from one equipotential surface to another along the lines of force from the charge source. The gradient is often given the symbol ∇, known as the *del*, and represents the operator $\left(\frac{\partial}{\partial x}, \frac{\partial}{\partial y}, \frac{\partial}{\partial z}\right)$. The gradient of a scalar field (e.g. Ψ) generates a vector. The gradient of the electrical potential Ψ is related to the electric field strength E in the following way

$$\mathrm{E} = -\nabla \Psi. \tag{3.2.1}$$

As the values of E vary from one position to another, they form a vector field with direction determined by the lines of force (Hunter, 1981).

The operator ∇ behaves like a vector and can form both a scalar (dot) product and a vector (cross) product. We can for instance take the scalar product of ∇ with the field strength E:

$$\nabla \cdot E = \frac{\partial E_x}{\partial x} + \frac{\partial E_y}{\partial y} + \frac{\partial E_z}{\partial z}. \tag{3.2.2}$$

This sum is invariant and the scalar product represents the flux per unit volume of the field strength E, which is referred to as the divergence of E (Feynman, Leighton, & Sands, 1965).

A common application of the divergence operator is the continuity equation, which shows that all material that flows into a given volume element also flows out, so the net flux of an incompressible fluid is zero:

$$\nabla \cdot v = 0, \tag{3.2.3}$$

where v represents the velocity of an incompressible fluid. The continuity equation can also be applied to E. The field strength, represented by the number of lines of force, is only affected by electric charges. Consequently, for a charge free region of space, the divergence of E is also zero. As discussed, E can be represented by the gradient of the scalar potential Ψ. We then achieve:

$$\nabla \cdot E = \nabla \cdot (-\nabla \Psi) = -\left(\frac{\partial}{\partial x}\left(\frac{\partial \Psi}{\partial x}\right) + \frac{\partial}{\partial y}\left(\frac{\partial \Psi}{\partial y}\right) + \frac{\partial}{\partial z}\left(\frac{\partial \Psi}{\partial z}\right)\right), \tag{3.2.4}$$

$$\nabla \cdot E = -\left(\frac{\partial^2 \Psi}{\partial x^2} + \frac{\partial^2 \Psi}{\partial y^2} + \frac{\partial^2 \Psi}{\partial z^2}\right) = -\nabla \cdot \nabla \, \Psi, \tag{3.2.5}$$

$$\nabla \cdot E = -\nabla^2 \, \Psi, \tag{3.2.6}$$

which in general would be a scalar, but in effect, the operator ∇ forms a scalar product with itself to produce a new scalar operator:

$$\nabla \cdot \nabla \equiv \nabla^2 = \frac{\partial^2}{\partial x^2} + \frac{\partial^2}{\partial y^2} + \frac{\partial^2}{\partial z^2}. \tag{3.2.7}$$

This operator is known as the Laplace operator or simply the Laplacian and means the divergence of the gradient (Feynman et al., 1965). As mentioned, for a charge free region of space, the divergence of E is zero. This is known as Laplace's equation:

$$\nabla^2 \Psi = 0. \tag{3.2.8}$$

A dielectric medium is an electrical insulator that reduces the strength of the electric field. When a dielectric material is subjected to an electric field, the molecular dipoles align themselves to cancel part of the field. Water is an example of a dielectric medium (Hunter, 1981). Permittivity is a materials capacity to affect (resist) the electric field strength, and is denoted by ε. High permittivity leads to reduced electric field (or electric flux) (Spencer & Moore, 2001). The dielectric displacement D, is introduced to account for the effects of permittivity:

$$D = \varepsilon E. \tag{3.2.9}$$

This is also known as the relative permittivity and can be expressed as

$$D = \varepsilon/\varepsilon_0, \tag{3.2.10}$$

where ε_0 is the permittivity *in vacuo*.

Gauss' law relates the electric charge density ρ to the electric field E. The law states that: *The net electric flux through any closed surface is equal to* $1/\varepsilon$ *times the net electric charge within that closed surface* (Serway, Beichner, & Jewett, 2000). The law can be written in the differential form:

$$\nabla \cdot E = \frac{\rho}{\varepsilon_0}. \tag{3.2.11}$$

If ε is assumed independent of spatial position, the corresponding equation for charges immersed in a dielectric medium (e.g. water) becomes

$$\nabla \cdot D = \rho \ \rightarrow \nabla \cdot \varepsilon E = \rho, \tag{3.2.12}$$

$$\nabla \cdot E = \frac{\rho}{\varepsilon}. \tag{3.2.13}$$

This equation was first developed by Lagrange in 1773, and later by Gauss in 1813. It is known as Gauss' law.

By combining equation (*3.2.6*) with Gauss' law, equation (*3.2.12*), we finally arrive at Poisson's equation:

$$\nabla \cdot E = div\, E = -\nabla^2 \Psi = \frac{\rho}{\varepsilon}, \tag{3.2.14}$$

$$\nabla^2 \Psi = -\frac{\rho}{\varepsilon}. \tag{3.2.15}$$

3.3. Electrical Double Layer

The charge development at a solid-liquid interface leads to formation of the electrical double layer (EDL). The electric field generated by the surface charge attracts counter ions from the liquid. The layer comprised of these charges and counter ions is known as the electrical double layer. It consists of two parallel layers of electric charge that surrounds the surface of the immersed object. The object may be a solid particle or particles, a porous medium, a bubble, or a droplet. In the following section, the theory of the electrical double layer independently developed by Gouy (1910) and Chapman (1913) is discussed as presented by, e.g. Butt (2006) and Hunter (1981).

The innermost part of the double layer is known as the Stern layer (sometimes referred to as the Helmholtz layer). The Stern layer consists of counter charges adsorbed on the solid surface. These charges are thus immobile, and the Stern layer has a limited thickness on the order of a molecular layer. The counter ions in the Stern layer do often not balance the surface charge on the solid. This gives rise to the formation of the outer part of the double layer.

The outer part of the EDL is called the Gouy-Chapman layer. The location and thickness of this layer is affected by the solid's electrical attraction of ions as well as the thermal diffusive motion that drives ions away from the solid. The difference between the inner and the outer layer is that the ions in the outer layer are not *attached* to the solid surface. This part of the EDL is more loosely connected to the solid-liquid interface, and is thus also known as the diffuse layer. As the electric forces from the surface charge compete against the diffusive forces in the liquid, the concentration of counter ions decrease with increasing distance from the solid surface. The outer boundary of the diffuse layer is where the fluid reaches electrical neutrality.

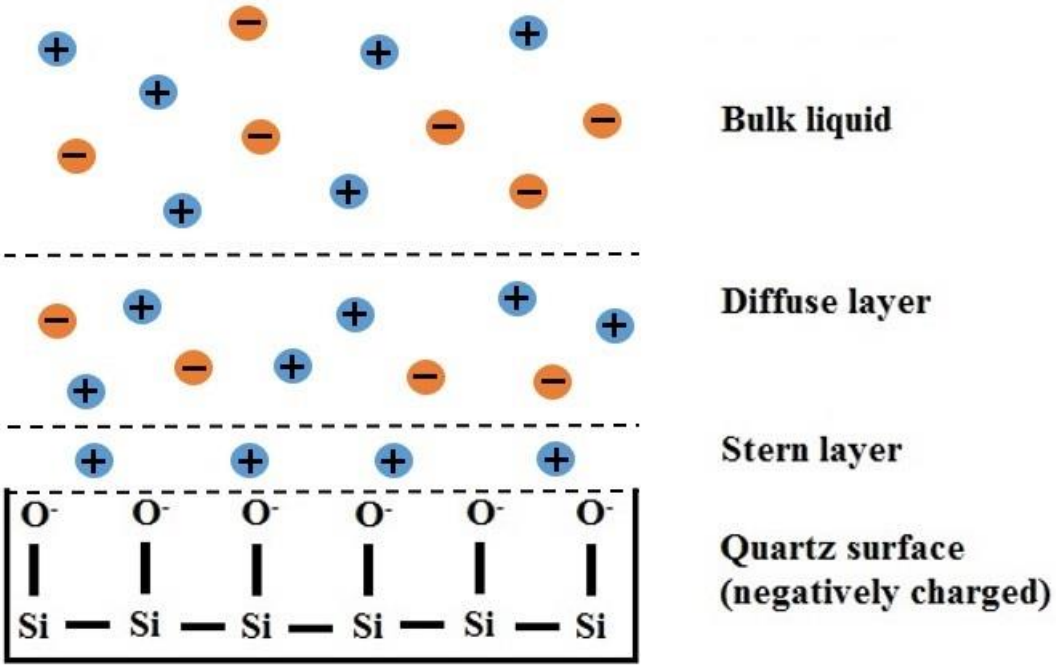

Figure 3.2 Simple illustration of the electrical double layer at static conditions, with negatively charged quartz surface. Ideally, the two regions of the EDL balance the surface charge on the solid such that the total electric charge remains neutral.

The effects of the electrical double layer become more significant as the pores/capillaries approach a scale of micro- to nanometres.

3.3.1. Electrical Double Layer for Flat Surfaces

In this section, the linearized form of Poisson's equation used to model the electrical double layer for flat surfaces is derived based on the work of Hunter (1981) and Feynman et al. (1965). In the model for flat surfaces, a charged planar interface is considered. It is assumed that the plate is immersed in an electrolyte with uniform surface charge density ρ. The surface charge creates an electric potential, which generally depends on the distance x, normal to the surface. The electric potential at the surface is thus $\Psi_0 = \Psi(x = 0)$. In the solution, the counter ions are regarded as point charges in a dielectric medium (as discussed in Chapter 3.2). The charge density ρ and the electric potential Ψ are related by Poisson's equation *(3.2.15)*:

$$\nabla^2\Psi = -\frac{\rho}{\varepsilon}. \tag{3.3.1}$$

The change in Gibbs free energy for a chemical system is:

$$dG = -SdT + Vdp + \bar{\mu}_i dn_i, \tag{3.3.2}$$

where $\bar{\mu}_i$ is the sum of the chemical potential and electrical potential: $\bar{\mu}_i = \mu + z_i e\Psi$ is the electrochemical potential and we for simplicity only consider one ion that in the initial state is far from a charged surface and in the final state close to the charged surface. We thus have for constant temperature, and pressure that:

$$\mu(x) + z_i e\Psi(\mathrm{x}) = \mu(\infty) + z_i e\Psi(\infty). \tag{3.3.3}$$

From the definition of chemical potential, where n_i is the number of ions of species i per unit volume (ion density), k_B is the Boltzmann constant and T is absolute temperature, we have

$$\mu_i = \mu_i^0 + k_B T \ln n_i \, . \tag{3.3.4}$$

This equation combined with equation *(3.3.3)* leads to the Boltzmann equation:

$$n_i = n_i^0 \cdot \exp\left(-\frac{z_i e\Psi}{k_B T}\right), \tag{3.3.5}$$

where $-z_i e\Psi$ represents the electric work needed to bring an ion in the solution from the bulk to a fixed position close to the surface. In other words, this equation describes the ion density at a specific position, as a function of the ion density in the bulk liquid, the absolute temperature, and the amount of electric work required to transport an ion from an arbitrary position in the bulk to the specific position.

If Ψ is negative (near a negatively charged surface), the concentration of cations at this position will be greater than in the bulk solution ($n_+ > n_+^0$), whereas the concentration of anions will be smaller ($n_- < n_-^0$).

The electric charge density ρ near the surface is given by the sum of the electric charge $Q = z_i \cdot e$ over all species of ions:

$$\rho = \textstyle\sum_i n_i z_i e. \tag{3.3.6}$$

By substituting for equations (*3.3.5*) and (*3.3.6*), and inserting in Poisson's equation (*3.3.1*), we arrive at the Poisson-Boltzmann equation:

$$\nabla^2\Psi = \frac{d^2\Psi}{dx^2} = -\frac{1}{\varepsilon} \cdot \textstyle\sum_i n_i^0 z_i e \cdot \exp\left(-\frac{z_i e\Psi}{k_B T}\right). \tag{3.3.7}$$

Note that the ∇^2-operator is simplified to one dimension due to the symmetry assumptions made earlier. Equation (*3.3.7*) is a non-linear differential equation, which can be solved analytically for the model for flat surfaces. However, it can be greatly simplified using the so-called Debye-Hückel approximation. This can be a useful tool for the Poisson-Boltzmann equation when solving for more complex geometries.

The Debye-Hückel approximation refers to the simplifying assumption that Ψ is small in magnitude. In this case, *small* means that $z_i e\Psi \ll k_B T$. Using the approximation $e^{-x} \approx 1 - x$ for small values of x, we see that

$$e^{-z_i e\Psi / k_B T} \approx 1 - \frac{-z_i e\Psi}{k_B T} = 1 + \frac{z_i e\Psi}{k_B T}.$$

Now, the summation term from equation (*3.3.7*) can be written

$$\sum_i n_i^0 z_i e \cdot \exp\left(-\frac{z_i e\Psi}{k_B T}\right) \approx \sum_i n_i^0 z_i e + n_i^0 z_i e \cdot \frac{z_i e\Psi}{k_B T}$$

$$= \sum_i n_i^0 z_i e + \sum_i n_i^0 \cdot \frac{z_i^2 e^2 \Psi}{k_B T},$$

and equation (*3.3.7*) is simplified to the linearized Poisson-Boltzmann equation:

$$\nabla^2 \Psi = \frac{d^2\Psi}{dx} = -\frac{1}{\varepsilon} \cdot \left(\sum_i n_i^0 z_i e + \sum_i n_i^0 \cdot \frac{z_i^2 e^2 \Psi}{k_B T}\right). \tag{3.3.8}$$

Due to the neutral electric charge in the bulk liquid, the first summation term must be zero. Hence, for the flat surface model, we can express the equation in the following way:

$$\nabla^2 \Psi = \frac{d^2\Psi}{dx} = \frac{-e^2 \sum_i n_i^0 \cdot z_i^2}{\varepsilon k_B T} \Psi.$$

A more common notation is

$$\nabla^2 \Psi = \frac{d^2\Psi}{dx} = \kappa^2 \cdot \Psi, \tag{3.3.9}$$

where

$$\kappa = \sqrt{\frac{e^2}{\varepsilon k_B T} \sum_i n_i^0 \cdot z_i^2}. \tag{3.3.10}$$

As this expression arises from the Debye-Hückel approximation, the parameter κ is known as the Debye-Hückel parameter. It has SI-unit m^{-1}, and mainly depends on the salt concentration n_i^0.

The length scale of the potential is given by κ^{-1}, and is referred to as the Debye length. The transition from the outer double layer to the bulk liquid is where the net charge becomes neutral, i.e. when the length $\gg \kappa$. As the Debye length is inversely proportional to the square root of the ion concentration, the electric potential Ψ decreases exponentially with distance x from the solid surface. This is illustrated in Figure 3.3 on page 23.

Depending on the ionic strength, κ^{-1} has values on the order of ~ 0.1 - 680 nm in aqueous solutions. κ increases with increasing salinity. An increase in κ leads to a more rapid decay of Ψ with distance, so the double layer is compressed with increasing ionic strength. The Debye length for a 0.1M NaCl solution is 0.96 nm, and it has a theoretical maximum of 680 nm in water because the ion concentration cannot decrease below $2x10^{-7}\ mol/L$ (Butt et al., 2006), because of the disassociation of H_2O in H^+ and OH^-. Practically, the Debye length ranges from 0.1 nm to 2 nm at reservoir conditions.

It is important to stress that the Debye-Hückel approximation is only valid for small values of Ψ. According to Butt et al. (2006), the approximation is generally valid for potentials up to 50-80 mV. In addition, the Debye length should not be interpreted as a *length* in the classical sense. It merely represents the scale of the EDL thickness.

3.4. Zeta Potential

So far in this chapter only static surface charge has been discussed. Now we will consider the dynamic case when a pressure difference is applied to induce fluid flow over the charged surface. With relative tangential motion between the solid and liquid, some of the ions in the EDL will start to slip. Ions in the Stern layer are adsorbed to the surface and will remain immobile. However, in the diffuse layer the charges can move more freely. The plane closest to the solid where the charges start to become mobile is referred to as the slipping plane, or perhaps more commonly the *shear plane*. This is a theoretical boundary which is believed to lie close to the solid surface, within the diffuse part of the double layer (Hunter, 1981). The average electrokinetic potential at the shear plane is known as the zeta potential (ζ potential). Figure 3.3 illustrates the location of the shear plane and zeta potential as well as the electric potential decay with respect to the electrical double layer at a negatively charged quartz surface.

The zeta potential is an important property to study because it can give valuable information about the electrical potential and surface charge of mineral surfaces. Electrostatic interactions between the surface and dissolved ions, between the surface and other charged interfaces, and between suspended particles are all controlled by the magnitude and sign of the zeta potential. In addition, experimental measurements of zeta potential are fairly straightforward compared to other methods for examining surface charge (Al-Mahrouqi, 2016).

Important factors that can affect the zeta potential primarily include pH and the ionic strength of the fluid. Gustafsson et al. (2000) showed that zeta potential decreases with increasing pH, although the effect becomes smaller as salinity increases. Also according to these experiments, zeta potential decreases with increasing salinity for pH lower than around 5.5, while the opposite is observed for pH values above 6.

Zeta potential can be determined experimentally by utilizing *electrokinetic phenomena*, such as electrophoresis and streaming potential measurements.

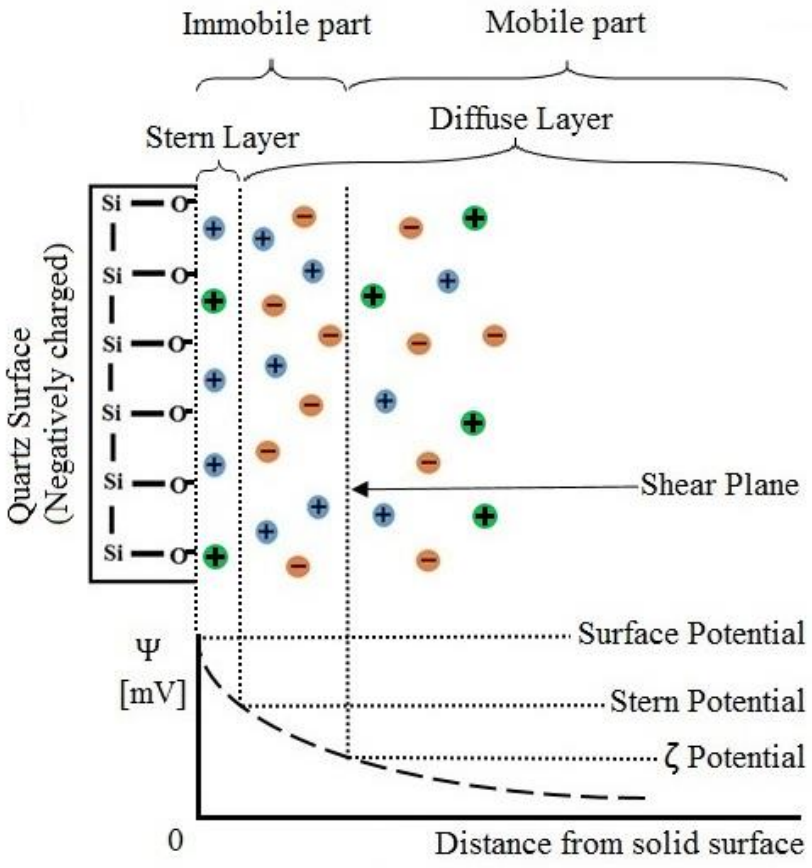

Figure 3.3 Illustration of zeta potential with respect to the shear plane and the electrical double layer for a quartz surface. The Stern layer can consist of different types of cations (marked green and blue).

Figure 3.3 illustrates the electrical double layer at a negatively charged mineral surface with the location of a shear plane and zeta potential. An immersed solid with negative surface charge will have a negative electrostatic potential with respect to the bulk fluid (Hunter, 1981). The potential will decrease until it becomes constant in the bulk fluid.

3.5. Electrokinetic Phenomena

Electrokinetic phenomena (EKP) are different effects arising from relative tangential motion between two phases (e.g. capillary tube or porous media). It typically refers to a solid-liquid interface, but electrical surface charge and double layers can also develop on liquid-liquid interfaces as long as both phases are polar or have polar components. However, electrokinetic effects at liquid-liquid interfaces are much less understood than those for solid-liquid interfaces (Al-Mahrouqi, 2016; Pascall & Squires, 2011). EKP can be divided into four distinct effects depending on the origin of the relative motion: *electro-osmosis*, *electrophoresis*, *sedimentation potential*, and *streaming potential* (Hunter, 1981). To achieve a more clear definition of electrokinetic phenomena, each of the four effects will be further explained, as presented by e.g. Lin et al. (2012) and Delgado et al. (2007).

Electro-osmosis: As an electric field is applied to a system consisting of a solid (in the form of a porous plug or a capillary) and a liquid, the liquid can start to flow. This process is called electro-osmosis. The electric field causes ions in the liquid to move, dragging the liquid with them. The liquid velocity per unit current flow can be measured to give information about the charge environment in the vicinity of the solid-liquid interface.

Electrophoresis: During electrophoresis, an electric field is applied to a fluid to induce flow through a porous plug or a capillary and the flow velocity is measured, similar to electro-osmosis. In this case the fluid has suspended solid or liquid particles. During electrophoresis the suspended particles in the fluid drags with them the fluid and thus the mobile charges close to the solid surface. The fluid velocity is normalized by E to yield the electrophoretic mobility $\mu_e = \frac{v}{E}$, which is related to the zeta potential by the Helmholtz-Smoluchowski equation for electrophoresis:

$$\mu_e = \frac{\varepsilon\,\zeta}{\eta}. \tag{3.5.1}$$

Sedimentation Potential: The electric potential difference generated as charged particles in a suspension settle under gravity, is called the sedimentation potential. The potential is detected by electrodes in the vertical direction. From the perspective of the particle, fluid is moving over the surface causing the atmosphere of mobile counter ions to be dragged in the direction of fluid flow. This creates a flow of counter ions in the opposite direction to the fluid flow.

Streaming Potential: During streaming potential measurements, a pressure difference Δp is applied to induce flow, and the resulting electric potential difference is measured. The process is similar to that for the sedimentation potential, only the fluid flow is induced by an external pressure difference. As the fluid flows over the solid surface, the mobile counter-ions are carried in the direction of fluid flow inducing a flow of charges in the opposite direction through the bulk of the fluid. The measured potential difference is related to the zeta potential by the Helmholtz-Smoluchowski equation for streaming potential (equation *(5.1.20)*):

$$E_s = \frac{\varepsilon\, \zeta\, \Delta p}{\eta\, \lambda}.$$

This can be derived from a combination of electrochemical equations and equations describing fluid flow, and will be discussed in more detail in Chapter 5.

Chapter 4. Fluid Flow

Electrokinetic phenomena combine the effects of electrochemistry and fluid flow. In this chapter, the motion of viscous fluid flow through a circular tube is described mathematically. The general Navier-Stokes equation is derived from first principles based on the work of Feynman et al. (1965) and Hunter (1981). Furthermore, Poiseuille's equation is derived as a special case of Navier-Stokes' equation, with support from White & Corfield (2006). The equations for viscous fluid flow will further be used in the derivation of the streaming potential equation in Chapter 5.

4.1. Navier-Stokes Equation

Navier-Stokes equation is a fundamental equation in fluid dynamics, used to describe viscous fluid flow. It is a balance equation that arises from Newton's second law of motion. The following derivation is based on the lectures of Feynman et al. (1965), and Hunter (1981), although here, electromagnetic forces are also considered. The basis of the derivation is the balance between the net force acting on a parcel of fluid and its mass times acceleration:

$$\sum F = m \cdot a. \tag{4.1.1}$$

However, in fluid dynamics it is often more convenient to divide the equation by volume and use the fluid density $D = \frac{m}{V}$:

$$\sum \frac{F}{V} = D \cdot [a], \tag{4.1.2}$$

where

$$[a] = \frac{a}{V}. \tag{4.1.3}$$

The acting forces discussed here will be the viscous drag force F_v, the driving pressure force (pressure gradient) F_p and the electromagnetic force F_e.

In the first case of this derivation, there are three assumptions to consider; we are dealing with laminar flow of a Newtonian fluid with no-slip boundary condition. Laminar flow means that the fluid velocity changes exclusively in y-direction (radially for a cylinder) as illustrated in Figure 4.1. The next assumption is the so-called no-slip condition. It is an important

experimental fact that the velocity of a fluid is exactly zero at the surface of a solid (for all ordinary fluids). This is also illustrated by the velocity profile of the laminar flow in Figure 4.1, where the velocity decreases to exactly zero at the interface between the fluid and the wall. The validity of these assumptions are briefly discussed in the end of this chapter.

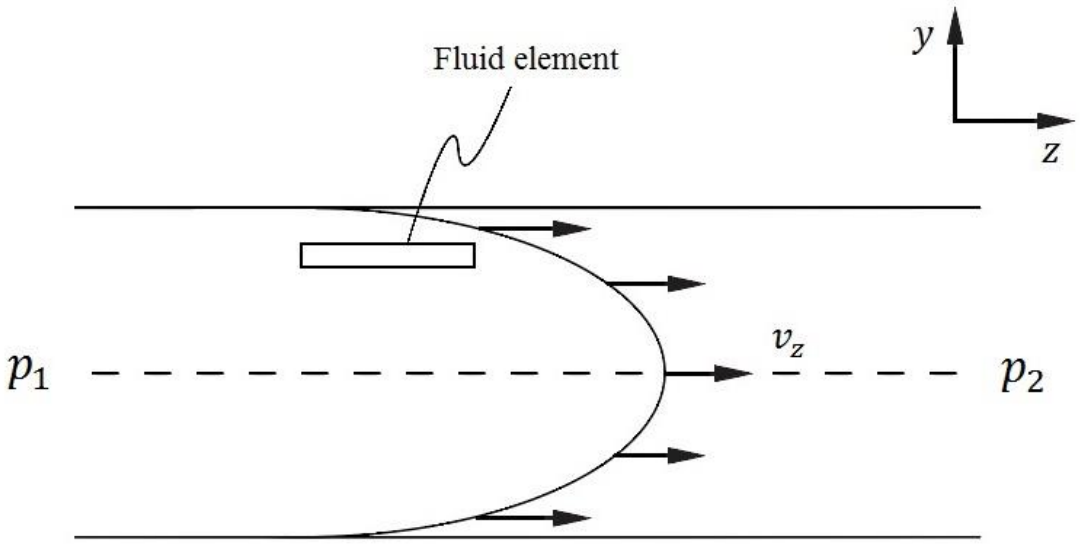

Figure 4.1 Illustration of the velocity profile for laminar flow of a Newtonian fluid. A fluid element is indicated, this is further described in Figure 4.2.

The first force to consider will be the viscous drag force. For a Newtonian fluid, the shear rate τ is proportional to the fluids viscosity η and can be expressed as a force divided by the area on which the force is acting:

$$\tau = \frac{F_v}{A} = -\eta \frac{\Delta v_z}{\Delta y}, \tag{4.1.4}$$

$$F_v = -A \cdot \eta \frac{\Delta v_z}{\Delta y}. \tag{4.1.5}$$

Where the viscous force is defined as negative as it opposes the fluid flow in positive z-direction. The fluid in Figure 4.1 can be divided in several fluid elements with different velocities. The area that the viscous shear force is acting on is then defined by $\Delta x \cdot \Delta z$ from Figure 4.2:

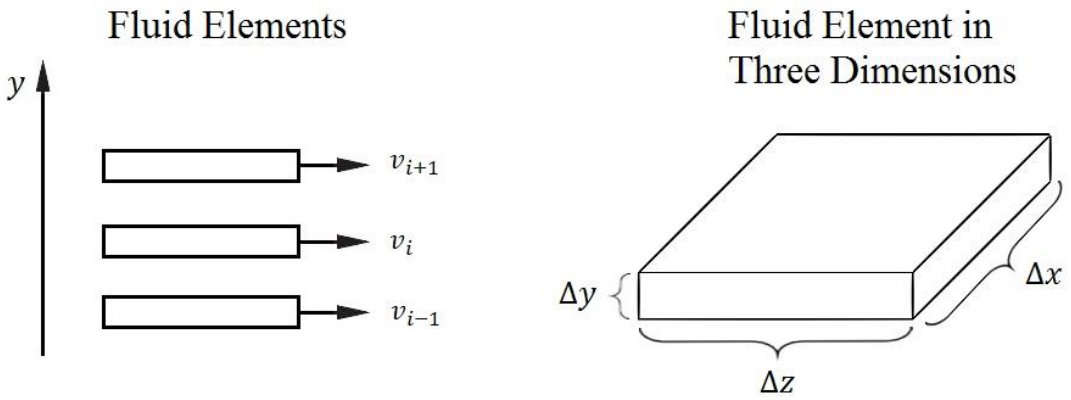

Figure 4.2 Left: Illustration of arbitrary fluid elements with associated velocities. Right: Definition of the dimensions of an arbitrary fluid element.

Hence, the viscous force can be expressed as

$$F_v = -\Delta x \cdot \Delta z \cdot \eta \frac{\Delta v_z}{\Delta y}, \tag{4.1.6}$$

$$F_v = -\Delta x \Delta z \, \eta \cdot \left(\frac{v_{i+1}-v_i}{\Delta y} + \frac{v_{i-1}-v_i}{\Delta y}\right), \tag{4.1.7}$$

where

$$\frac{v_{i+1}-v_i}{\Delta y} + \frac{v_{i-1}-v_i}{\Delta y} = \frac{v_{i+1}-2v_i+v_{i-1}}{\Delta y} = \Delta y \frac{d^2v}{dy^2}. \tag{4.1.8}$$

Furthermore, this can be series expanded using *Taylor expansion* on the form

$$f(x+\Delta x) = f(x) + \frac{1}{1!}f'(x) \cdot \Delta x + \frac{1}{2!}f''(x) \cdot \Delta x^2 + \cdots \tag{4.1.9}$$

Applying the Taylor expansion to the expressions for v_{i+1} and v_{i-1} gives

$$v_{i+1} = v(y+\Delta y) = v(y) + \frac{dv}{dy}\Delta y + \frac{1}{2}\frac{d^2v}{dy^2}\Delta y^2 + \cdots \tag{4.1.10}$$

$$v_{i-1} = v(y-\Delta y) = v(y) - \frac{dv}{dy}\Delta y + \frac{1}{2}\frac{d^2v}{dy^2}\Delta y^2 + \cdots \tag{4.1.11}$$

The general expression for the viscous forces F_v becomes

$$F_v = -\Delta x \Delta y \Delta z \, \eta \frac{d^2v}{dy^2}. \tag{4.1.12}$$

Expressed as force per unit volume, this becomes

$$\frac{F_v}{V} = -\eta \nabla^2 v. \tag{4.1.13}$$

The fluid flow is driven by the pressure difference Δp between p_1 and p_2 (Figure 4.1). Again, the fluid is divided in fluid elements as illustrated in Figure 4.2 and Figure 4.3. The driving pressure acts on the area defined by $\Delta x \cdot \Delta y$ for each fluid element. Consequently, the total pressure force acting on the fluid can be expressed as

$$F_p = \Delta x \Delta y \Delta p. \tag{4.1.14}$$

Note that the driving pressure force is defined as positive as it induces the fluid flow in positive z-direction. Again, expressed as force per unit volume, the equation becomes

$$\frac{F_p}{V} = \nabla p. \tag{4.1.15}$$

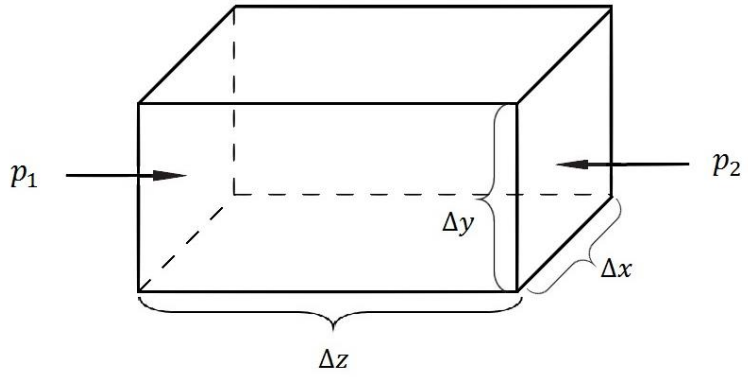

Figure 4.3 Three-dimensional fluid element with pressure difference $\Delta p(z) = p_1 - p_2$ indicated.

Along with the pressure and viscous forces, we shall also consider the electromagnetic effects. The force per unit volume is given in terms of the electric potential and charge density by

$$\frac{F_e}{V} = \rho \nabla \Psi. \tag{4.1.16}$$

All forces acting on the fluid can now be added and inserted in Newton's law of motion for fluid flow *(4.1.2)*:

$$\frac{1}{V}(F_v + F_p + F_e) = D \cdot [a], \tag{4.1.17}$$

$$-\eta \nabla^2 v + \nabla p + \rho \nabla \Psi = D \cdot [a]. \tag{4.1.18}$$

For laminar flow, the inertial term $D \cdot [a]$ will be zero because there is no acceleration of the bulk fluid nor of any particle in the fluid (centripetal acceleration). However, the general form of the Navier-Stokes equation considers inertial forces, so the next step will be to find an expression for the total fluid acceleration.

The normal acceleration notation $\frac{\partial v}{\partial t}$ refers to velocity changes for a fixed position in space. We are interested in the change in particle velocity. During a time step Δt, a particular particle moves a distance of $\Delta x = v_x \Delta t$ in x-direction, $\Delta y = v_y \Delta t$ in y-direction, and $\Delta z = v_z \Delta t$ in z-direction. If the velocity of the fluid particle at position (x, y, z) and time t is $v(x, y, z, t)$, the particle velocity is given by $v(x + \Delta x, y + \Delta y, z + \Delta z, t + \Delta t)$ (Butt et al., 2006). With the given expressions for Δx, Δy and Δz, the particle velocity can be expressed as

$$v\big(x + v_x \Delta t, y + v_y \Delta t, z + v_z \Delta t\big)$$

$$= v(x, y, z, t) + \frac{\partial v}{\partial x} v_x \Delta t + \frac{\partial v}{\partial y} v_y \Delta t + \frac{\partial v}{\partial z} v_z \Delta t + \frac{\partial v}{\partial t} \Delta t. \tag{4.1.19}$$

Furthermore, dividing the velocity by Δt gives the particle acceleration:

$$a = \frac{\Delta v}{\Delta t} = v_x \frac{\partial v}{\partial x} + v_y \frac{\partial v}{\partial y} + v_z \frac{\partial v}{\partial z} + \frac{\partial v}{\partial t}, \tag{4.1.20}$$

which can be written

$$a = (v \cdot \nabla) v + \frac{\partial v}{\partial t}, \tag{4.1.21}$$

using the gradient notation.

The importance of distinguishing between the fixed space acceleration and the particle acceleration becomes clear from equation *(4.1.21)*. There can be a particle acceleration even if $\frac{\partial v}{\partial t} = 0$, but only for rotational acceleration (centripetal acceleration), which can occur during turbulent flow. Hence, the inertial term for the general case becomes:

$$D \cdot [a] = D \left[(v \cdot \nabla) v + \frac{\partial v}{\partial t} \right]. \tag{4.1.22}$$

By combining equations *(4.1.18)* with *(4.1.22)*, we achieve a general expression of the Navier-Stokes equation:

$$-\eta \nabla^2 v + \nabla p + \rho \nabla \Psi = D \left[(v \cdot \nabla) v + \frac{\partial v}{\partial t} \right]. \tag{4.1.23}$$

4.2. Poiseuille's Equation

Poiseuille's equation gives an exact solution to the Navier-Stokes equation, assuming axisymmetric, fully developed steady state flow with no-slip boundary condition. The following derivation is thus based on Navier-Stokes, in addition to the derivation presented by White & Corfield (2006). Poiseuille flow refers to laminar flow through a circular tube. This is illustrated in Figure 4.4.

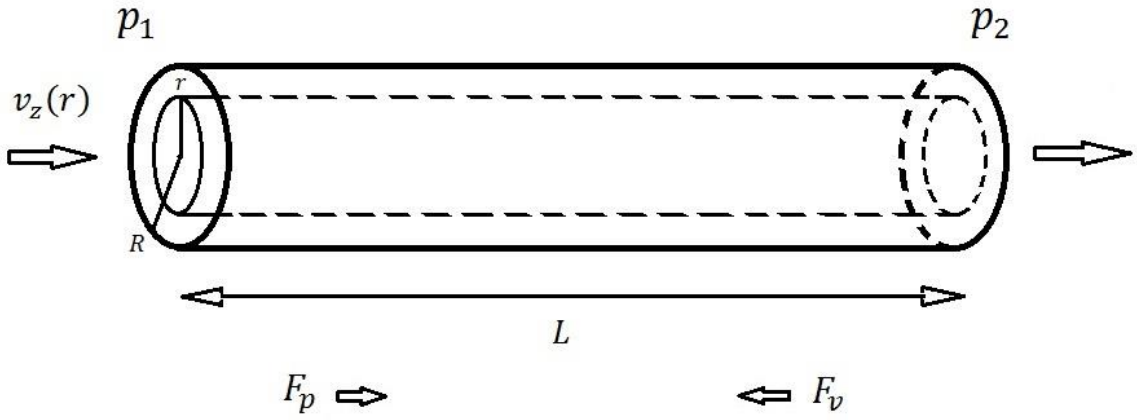

Figure 4.4 Capillary tube with length and radius indicated in addition to pressure difference, flow direction and direction of the pressure force and viscous force.

For steady state laminar flow in a capillary tube for electrokinetic problems, the acceleration at a point in the fluid is zero and there is no centripetal acceleration, so the sum of all forces acting on a fluid element will add to zero: $F_v + F_p + F_e = 0$. Consequently, the general form of the Navier-Stokes equation *(4.1.23)* for this special case reduces to

$$-\eta\nabla^2 v + \nabla p + \rho\nabla\Psi = 0. \tag{4.2.1}$$

Since the fluid velocity only varies in z-direction, we can write

$$-\eta\frac{d^2v}{dr^2} + \frac{\Delta p}{L} + \rho\nabla\Psi = 0, \tag{4.2.2}$$

$$\frac{d^2v}{dr^2} = \frac{\Delta p}{\eta L} + \frac{\rho}{\eta}\nabla\Psi, \tag{4.2.3}$$

in cylindrical coordinates. Integrating equation *(4.2.3)* twice provides an expression for the fluid velocity $v_z(r)$ in the capillary tube:

$$\int_0^v\int_0^v d^2v = \int_r^R\int_0^r\left(\frac{\Delta p}{\eta L} + \frac{\rho}{\eta}\nabla\Psi\right)dr^2, \tag{4.2.4}$$

$$v_z(r) = \left(\frac{\Delta p}{L} + \rho \nabla \Psi\right) \frac{(R^2 - r^2)}{4\eta}. \tag{4.2.5}$$

Equation *(4.2.5)* is a parabolic equation that expresses the linear fluid velocity in z-direction as a function of distance r from the axis of the capillary tube. Figure 4.5 below illustrates the velocity gradient and the corresponding velocity profile.

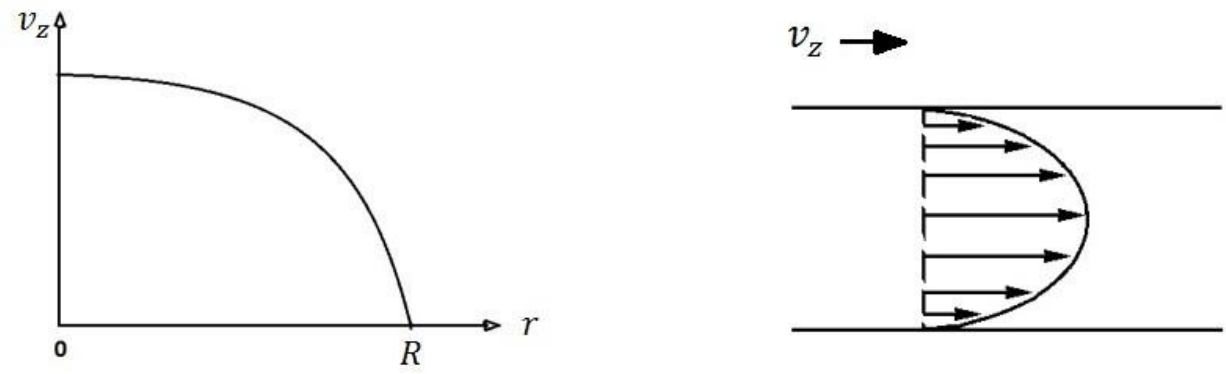

Figure 4.5 Left: The velocity gradient as expressed by equation (4.2.5). Right: The corresponding velocity profile in a tube.

Poiseuille's equation is expressed by volumetric flow rate q. In this case, the volumetric flow rate $\frac{dV}{dt} = q$ is calculated by integrating the fluid velocity over the radius with respect to the cross sectional area of the cylinder:

$$\frac{dV}{dt} = \int v_z(r)\, dA, \tag{4.2.6}$$

where

$$dA = \frac{d}{dr}(\pi r^2) = 2\pi r dr, \tag{4.2.7}$$

and

$$v_z(r) = \left(\frac{\Delta p}{L} + \rho \nabla \Psi\right) \frac{(R^2 - r^2)}{4\eta},$$

from equation *(4.2.5)*. The following result is achieved:

$$\frac{dV}{dt} = \int_0^R \left(\frac{\Delta p}{L} + \rho \nabla \Psi\right) \frac{(R^2 - r^2)}{4\eta}\, 2\pi r dr, \tag{4.2.8}$$

$$\frac{dV}{dt} = \left(\frac{\Delta p}{L} + \rho \nabla \Psi\right) \frac{\pi}{2\eta} \int_0^R (R^2 r - r^3)\, dr = \left(\frac{\Delta p}{L} + \rho \nabla \Psi\right) \frac{\pi}{2\eta} \left(\frac{R^4}{2} - \frac{R^4}{4}\right), \tag{4.2.9}$$

$$\frac{dV}{dt} = \frac{\pi R^4}{8\eta} \left(\frac{\Delta p}{L} + \rho \nabla \Psi\right) = q. \tag{4.2.10}$$

This is Poiseuille's equation for laminar fluid flow in a capillary tube, accounting for electromagnetic forces as well as viscous forces and the pressure gradient. It can alternatively be expressed by the pressure difference Δp:

$$\Delta p = \frac{8\eta L q}{\pi R^4} - L\rho\nabla\Psi. \tag{4.2.11}$$

A few simple assumptions were made to reach the expression for Poiseuille flow. As mentioned in chapter 4.1, the no-slip condition is confirmed by a large number of experiments for ordinary fluids at pressures of around one atmosphere and larger (Lauga, Brenner, & Stone, 2007). It essentially means that adhesion is stronger than cohesion for particles close to the surface. For the assumption of laminar flow to be correct, the Reynolds number for the flow situation should be less than 1000 (Holman, 2002). The Reynolds number is the ratio between inertial forces and viscous forces and is defined as

$$R_e = \frac{Dvd}{\eta}, \tag{4.2.12}$$

where D: fluid density, v: fluid velocity, d: grain diameter and η: dynamic viscosity. With some typical values from reservoirs on the Norwegian continental shelf

$$D = 1000\ kg/m^3, v = 1\ m/day \approx 10^{-5}\ m/s, d = 10^{-6}\ m, \eta = 10^{-3}\ Pa \cdot s,$$

The Reynolds number can be calculated to leading order:

$$R_e = \frac{10^3 \cdot 10^{-5} \cdot 10^{-6}}{10^{-3}} = 10^{-5} \ll 1000. \tag{4.2.13}$$

This confirms that the assumption of laminar flow is valid for this flow situation. At the start of fluid flow, or when a flowing fluid enters a tube, the velocity profile associated with laminar flow takes some time establishing. Fully developed flow is reached when the velocity profile remains constant.

Chapter 5. Streaming Potential

In this chapter we show that, at the interface between a charged phase (often a solid) and an electrolyte, a measurable electric potential difference can be set up by the flow of fluid induced by a pressure difference. To achieve an understanding of the concepts, single phase streaming potential is first considered. The established theory on this subject is presented, as well as the derivation of Helmholtz-Smoluchowski's equation for single phase streaming potential from Poiseuille's equation and Poisson's equation. Furthermore, some recent theory on two-phase streaming potential is discussed. This includes simple mathematical models developed by Sherwood (2007) to predict how the streaming potential is affected by an oil phase. This lays the final foundation for the analysis of the models and experimental results that will be discussed in Chapter 6.

5.1. Single Phase Streaming Potential

Streaming potential is the resulting potential difference that arises when a pressure difference Δp is applied to induce flow in a capillary or porous media with a charged surface, at zero net current. When a solid surface is immersed in a dielectric fluid a layer of surface charge, and consequently an electrical double layer, is developed at the interface. As the fluid flows over the solid surface, some of the mobile ions in the diffuse part of the double layer are carried in the direction of fluid flow. I.e. the fluid flow establishes a streaming current along the shear plane in the EDL. As the charges are *pulled* away from their initial location, they eventually slip back into place through the bulk of the fluid. This generates an electric conduction current in the opposite direction of the streaming current. At equilibrium, the resulting electrostatic potential difference can be measured across the capillary or plug. This potential difference is termed the streaming potential (Delgado et al., 2007; Hunter, 1981; Revil, Schwaeger, Cathles, & Manhardt, 1999).

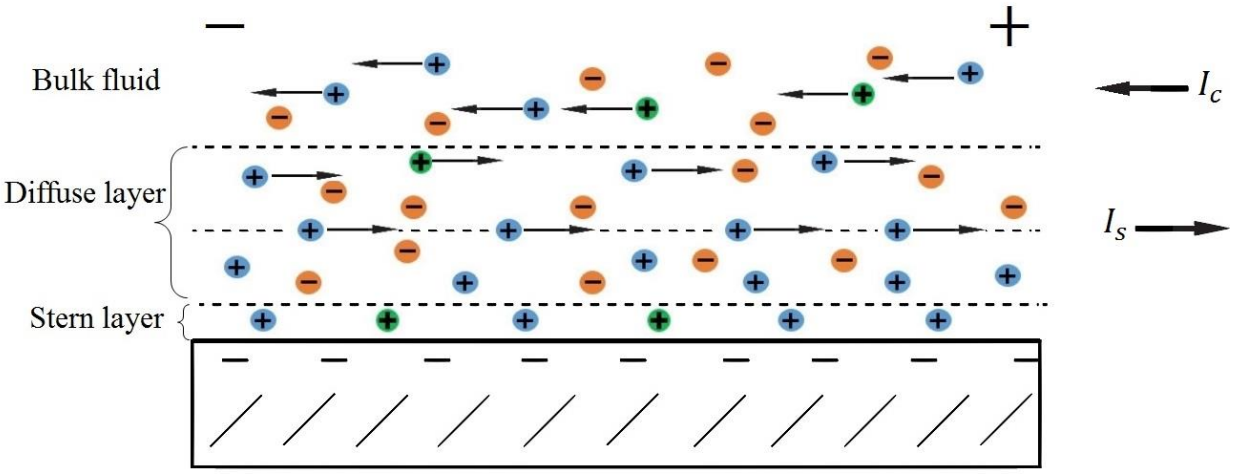

Figure 5.1 Illustration of streaming potential. The streaming current I_s forms in the EDL in the direction of fluid flow. The conduction current I_c moves in the opposite direction through the bulk fluid. Total measured electric potential is the streaming potential.

Streaming potential can be measured experimentally both in a lab and downhole in a well (Chen, Raghuraman, Bryant, & Supp, 2006). During lab measurements, a core sample is fitted inside a rubber sleeve with one electrode on each side. The core is flooded with a brine at constant rate or constant pressure. The electric potential difference between the two electrodes (the streaming potential) is registered. The streaming potential E_s is often plotted against the pressure difference Δp to determine the streaming potential coupling coefficient C_{sp}, which is defined as $C_{sp} = \frac{E_s}{\Delta p}$ (This is further discussed in Chapter 5.1.1). Laboratory measurements of streaming potential can be performed both for single phase and multi-phase flow (Al-Mahrouqi, 2016; Jackson, Vinogradov, Saunders, & Jaafar, 2011).

Successful field measurements of streaming potential was first conducted in 2006 by (Chen et al.). Electrodes placed in the borehole measured streaming potential arising from pressure transients. The field measurements can be used to monitor the water front during production and to create a geometric model of the moving fluid fronts. Jackson (2011) showed that SP measurements can detect moving water fronts at a significant distance (on the order of 100 m) from the producing well.

Streaming potential measurements can also for instance be utilized to estimate the wetting preference of a petroleum reservoir. The streaming potential can be used to determine the average zeta potential of the rock surface. Since the zeta potential is the electric potential at the shear plane, and there is a difference in zeta potential for the different fluids, the average zeta potential of the rock can offer reliable information on the wetting state of the rock surface

(Rahbar et al., 2017). Al-Mahrouqi (2016) found a linear regression between the zeta potential from streaming potential measurements and the Amott water-wetting index for all five types of natural crude oils tested.

Streaming potential measurements also have other practical applications. E.g. SP measurements can detect gas-liquid interfaces during seismic. Seismic waves generate electrical signals that may be larger near a gas-liquid interface. The compressibility of the gas causes enhanced relative motion between the gas and rock, and the resulting electric signal can be detected by sensors (Chandler, 1981). Furthermore, Xie et al. (2011) have looked at the possibility of using two-phase SP for electric power generation.

There are some factors that can affect streaming potential measurements. The effect of surface conductivity is important to consider. If the surface conductivity of the capillary or porous medium is high, some of the conduction current will be transported within the electrical double layer close to the solid surface (Shaw, 1980). This can disrupt the streaming potential measurements. The effect of surface conductivity is most likely to affect measurements for low electrolyte concentrations, when the EDL is thick. Overlapping double layers can also cause problems for SP measurements. Double layer overlap may appear for sufficiently small capillary radii or thick EDLs. In this case, the transport of ions will be partially prevented, which will reduce the measured streaming potential (Ban, Lin, & Song, 2010; Butt et al., 2006). Clay particles in the formation have been shown to restrict movement of anions, and thereby affect the measured streaming potential (Appelo & Wersin, 2007).

5.1.1. Helmholtz-Smoluchowski's Equation for Single Phase Streaming Potential

Streaming potential for single phase flow can be described by Helmholtz-Smoluchowski's equation. This equation combines the effects of fluid flow and electrostatic forces. It can be derived from Poiseuille's equation for laminar fluid flow as a special case of the Navier-Stokes equations, in combination with Poisson's equation for electrostatics. The following derivation is based on the work of Hunter (1981). As shown in chapter 4.2, Poiseuille's equation *(4.2.5)* for linear fluid velocity in a capillary tube is

$$v_z(r) = \frac{\Delta p}{4\eta L}(R^2 - r^2), \tag{5.1.1}$$

where r is the distance from the axis of the capillary tube, R is the radius of the tube, L is the length of the tube, η is dynamic fluid viscosity and Δp is the pressure drop. For the sake of simplicity, the small effect of electromagnetic forces are now neglected.

The streaming current I_s arises from the movement of mobile ions in the diffuse part of the double layer and is defined as

$$I_s = \int_{volume} v_z(r) \cdot \rho(r)\, dV, \tag{5.1.2}$$

$$I_s = \int_0^R 2\pi r \cdot v_z(r) \cdot \rho(r)\, dr, \tag{5.1.3}$$

where $\rho(r)$ is the charge density from Poisson's equation (*3.2.15*).

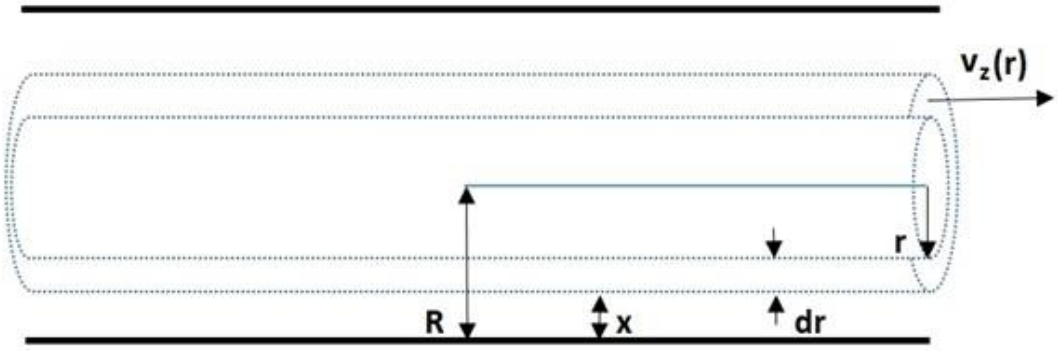

Figure 5.2 Fluid flow in a capillary tube. For simplicity reasons, x denotes the distance from the capillary wall. Modified from Hunter (1981).

The double layer is assumed restricted to a thin region near the wall of the capillary tube and the bulk fluid carries no net charge. Hence, only values of r close to R are relevant for determining the streaming current I_s. For simpler notation in the following derivation, the Debye length κ^{-1} is here denoted by x as in Figure 5.2. This allows us to substitute $r = (R - x)$. We then achieve

$$R^2 - r^2 = 2Rx - x^2. \tag{5.1.4}$$

Consequently, the Poiseuille equation for fluid velocity *(5.1.1)* becomes

$$v_z = \Delta p \cdot \frac{2Rx - x^2}{4\eta L}. \tag{5.1.5}$$

Since $x \ll R$, we can express v_z as

$$v_z \approx \frac{\Delta p R x}{2\eta L}. \tag{5.1.6}$$

Furthermore, I_s becomes

$$I_s = -\frac{\pi \Delta p R}{\eta L} \int_R^0 (R - x) \cdot x \cdot \rho(x)\, dx. \tag{5.1.7}$$

Again based on the assumption $x \ll R$, we have

$$\frac{\pi \Delta p R}{\eta L}(R - x) \approx \frac{\pi \Delta p R}{\eta L} R, \tag{5.1.8}$$

which leads to

$$I_s \approx -\frac{\pi \Delta p R^2}{\eta L} \int_R^0 x \cdot \rho(x)\, dx, \tag{5.1.9}$$

where $\rho(x)$ from Poisson's equation *(3.2.15)* is

$$\rho(x) = -\varepsilon\, \nabla^2 \Psi = -\varepsilon\, \frac{d^2\Psi}{dx^2}. \tag{5.1.10}$$

Next, substituting for $\rho(x)$ in equation *(5.1.9)* yields

$$I_s = \frac{\pi \Delta p R^2}{\eta L} \int_R^0 x\, \varepsilon \frac{d^2\Psi}{dx^2}\, dx. \tag{5.1.11}$$

This equation can be solved from integration by parts:

$$I_s = \frac{\pi \Delta p R^2 \varepsilon}{\eta L} \left(\left[x \frac{d\Psi}{dx} \right]_R^0 - \int_R^0 \frac{d\Psi}{dx}\, dx \right), \tag{5.1.12}$$

where $x \frac{d\Psi}{dx} = 0$ for both limits. Next, the electric potential is integrated from 0 to ζ

$$I_s = -\frac{\pi \Delta p R^2 \varepsilon}{\eta L} \int_0^\zeta d\Psi, \tag{5.1.13}$$

$$I_s = -\frac{\varepsilon\, \zeta}{\eta L}\, \pi \Delta p R^2. \tag{5.1.14}$$

The conduction current is the flow of electrons through the bulk fluid due to potential difference created by the streaming current. Consequently, the two currents act in opposite directions. The conduction current is given by Ohm's law

$$I_c = A\lambda \frac{\Delta V}{L}, \tag{5.1.15}$$

where A is the cross-sectional area, L is the capillary length and ΔV is the streaming potential difference E_s:

$$I_c = \frac{\pi R^2 E_s \cdot \lambda_0}{L} + \frac{2\pi R E_s \cdot \lambda_s}{L}. \tag{5.1.16}$$

Here, λ_0 is the bulk conductivity and λ_s is the surface conductivity.

At steady state conditions, the streaming- and conduction currents are equal in magnitude, acting in opposite directions:

$$\frac{\varepsilon\,\zeta}{\eta L} \cdot \pi \Delta p R^2 = \frac{\pi R^2 \lambda_0}{L} \cdot E_s + \frac{2\pi R \lambda_s}{L} \cdot E_s. \tag{5.1.17}$$

By solving for E_s, we achieve the equation known as the Helmholtz-Smoluchowski equation:

$$E_s = \frac{\varepsilon \zeta \Delta p}{\eta\left(\lambda_0 + 2\frac{\lambda_s}{R}\right)}. \tag{5.1.18}$$

The streaming potential E_s is often normalized by Δp to give the streaming potential coupling coefficient

$$C_{SP} = \frac{E_s}{\Delta p} = \frac{\varepsilon\,\zeta}{\eta\left(\lambda_0 + 2\frac{\lambda_s}{R}\right)}, \tag{5.1.19}$$

which is frequently used when determining the zeta potential from experimental measurements.

A common simplification is to neglect the surface conductivity λ_s. Alkafeef & Alajmi (2006) argued that this is valid if the fluid conductivity is high ($> 0.6\ S/m$), or if the thickness of the EDL (κ^{-1}) is less than the characteristic radius of curvature. Briggs (1928) assumed that effects of surface conductivity is negligible for electrolyte concentrations over $0.1\ mol/l$. If this simplification is made, the Helmholtz-Smoluchowski equation can be expressed in the simpler form:

$$E_s = \frac{\varepsilon\,\zeta\,\Delta p}{\eta\,\lambda}. \tag{5.1.20}$$

In this case, the streaming potential coupling coefficient of course also reduces to

$$C_{SP} = \frac{\varepsilon\,\zeta}{\eta\,\lambda}. \tag{5.1.21}$$

5.2. Two-Phase Streaming Potential

Streaming potential caused by single phase aqueous fluids in capillaries and porous media are reasonably well understood. However, the interpretation of streaming potential measurements in the presence of an oil phase is much more complicated. To deal with this, model problems need to be considered. A few mathematical models have been developed in recent years. The most relevant ones for this thesis are the analytical model of a charged spherical particle in the centre of a water-wet capillary tube and the similar model for an uncharged spherical bubble, both developed by Sherwood (2007).

Jackson (2008) considers a bundle of tubes model for investigating the effect of streaming potential. In the bundle of tubes model the porous media is represented as a distribution of circular tubes with different radii. In a water wet system, oil invades the largest pores first and the water resides in the smaller pores. The coupling coefficient in this case for a water-wet system is independent of saturation. This is because in the bundle of tubes model, the fluid configurations are trivial. As the capillaries are filled with oil the relative permeability for water drops, and the streaming potential decreases correspondingly. The model of Jackson (2008) is relevant for the case where two fluids flow at the same time. In this thesis we are more concerned with understanding the effect of the zeta potential when primarily water is flowing. In Al-Mahrouqi (2016), there is a claim that a change in the streaming potential is an indication of wettability change. Clearly, if oil is removed from the rock surface, the surface charge increases and the streaming potential will increase. But, if oil is slowly released as small droplets, can the presence of the oil phase itself gives observable changes in the streaming potential? In the following we will use the model of Sherwood (2007) to investigate this further.

In addition to the models, experimental results and correlations can help us develop a better understanding of two-phase streaming potentials. Important experimental studies include those of Al-Mahrouqi (2016) and Rahbar et al. (2017). Both found an experimental correlation between measured streaming potential and rock wettability. In the following sections the models and experimental results will be presented and analysed in an effort to determine how the presence of an oil phase affects streaming potential measurements in relation to saturation and wettability.

5.2.1. Single Spherical Droplet in a Capillary

The model problem *(i)* presented by Sherwood (2007) considers a close-fitting rigid spherical particle in a circular capillary. The Debye length κ^{-1} is assumed much smaller than the minimum gap width h_0 between the particle and the capillary wall. The particle is mobile and moves along the centreline of the capillary in response to the applied pressure difference Δp. The particle may represent a second fluid phase such as oil, or it could be a solid particle. This simple model attempts to predict the streaming potential as function of saturation in a water-wet capillary. In the following, a compressed version of the model derivation is presented, and the original author points out that the following analysis is valid only to leading order. The derivation generally follows the same procedure as in Chapter 5.1.1.

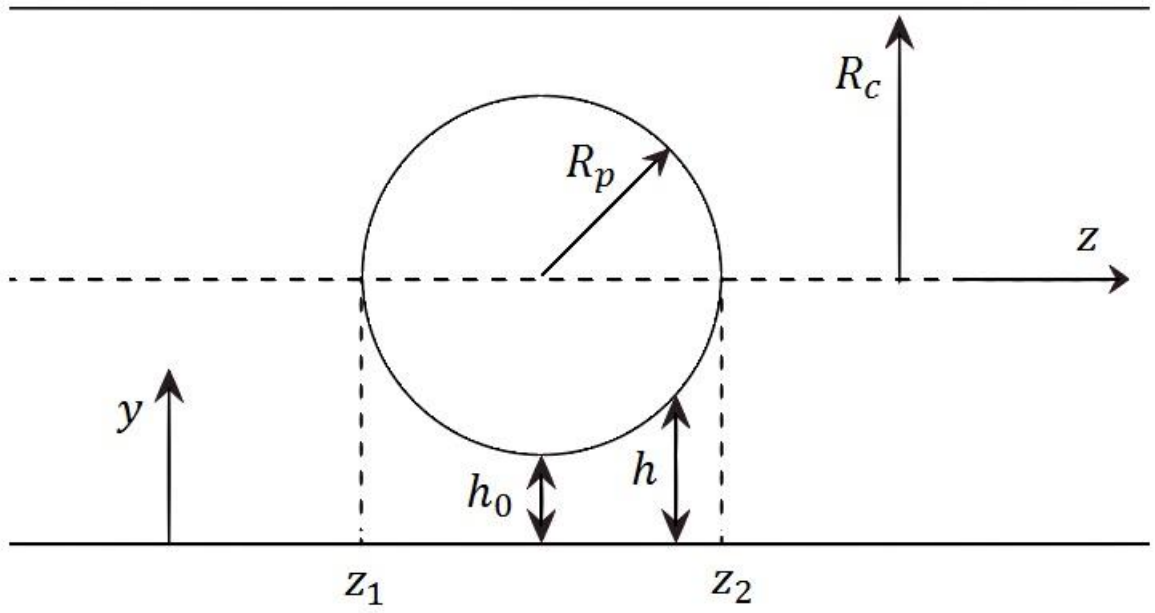

Figure 5.3 Illustration of the spherical particle of radius R_p in a capillary of radius $R_c = R_p + h_0$. Lengths are not to scale. Modified from Sherwood (2007).

It is assumed that the fluid flow can be described by Poiseuille's equation as the previous case. From Chapter 4.2, we have Poiseuille's equation for fluid flow without any particle:

$$\Delta p_w = \frac{8\eta L q}{\pi R_c^4} = \frac{8\eta L v}{R_c^2}. \tag{5.2.1}$$

Expressed by the capillary radius R_c, not accounting for any electromagnetic forces.

When the particle is present, we need to consider the total pressure drop over the sphere in addition to the pressure drop along the capillary. With the sphere centre located at $z = 0$, the gap between the sphere and the capillary wall can be expressed as:

$$\left(h(y) - \left(R_p + h_0\right)\right)^2 + z^2 = R_p^2, \tag{5.2.2}$$

$$h(y) - \left(R_p + h_0\right) = -\sqrt{R_p^2 - z^2}, \tag{5.2.3}$$

$$h(y) = R_p + h_0 - \sqrt{R_p^2 - z^2}, \tag{5.2.4}$$

where the last term can be series-expanded to

$$\sqrt{R_p^2 - z^2} = R_p\left(1 - \frac{1}{2}\left(\frac{z}{R_p}\right)^2 + \cdots\right). \tag{5.2.5}$$

This leads to the following expression for the gap width

$$h(y) = h_0 + \frac{z^2}{2R_p} + \cdots = h_0\left(1 + \frac{z^2}{d^2} + \cdots\right), \tag{5.2.6}$$

where

$$d = \sqrt{2R_p h_0}. \tag{5.2.7}$$

We define a coordinate system that follows the particle, such that the capillary wall moves with a velocity of $-v$. The steady state Navier-Stokes equation takes the form

$$\frac{d^2 v_p}{dy^2} = \frac{G}{\eta}. \tag{5.2.8}$$

Since this is a rigid particle, the no-slip boundary condition can be utilized:

$$v_p(0) = -v, \tag{5.2.9}$$

$$v_p(h) = 0. \tag{5.2.10}$$

Thus, Navier-Stokes equation can be integrated:

$$v_p(y) = \frac{G}{\eta}\frac{1}{2}y^2 + Cy + D. \tag{5.2.11}$$

From the boundary conditions, we achieve

$$D = -v, \tag{5.2.12}$$

and

$$C = \frac{1}{h}\left(v - \frac{G}{2\eta}\, h^2\right). \tag{5.2.13}$$

Consequently, the particle velocity becomes

$$v_p = \frac{G}{2\eta} y(y-h) + \frac{v}{h}(y-h). \tag{5.2.14}$$

This leads to the following equation for the flux through the gap between the particle and capillary wall:

$$q_p = 2\pi \int_{y=0}^{h} (R_c - y) v_p \, dy, \tag{5.2.15}$$

$$q_p = 2\pi \int_{0}^{h} \left((R_c - y) \frac{G}{2\eta} \, y(y-h) + (R_c - y)(y-h) \frac{v}{h} \right) dy, \tag{5.2.16}$$

$$q_p = -2\pi \left(\frac{G}{\eta} \left(\frac{h^3 R_c}{12} - \frac{h^4}{24} \right) + U \left(\frac{R_c h}{2} - \frac{h^2}{6} \right) \right). \tag{5.2.17}$$

Furthermore, this equation can be solved for G to achieve an expression for the pressure drop over the sphere:

$$\frac{q_p}{-2\pi} - v \left(\frac{R_c h}{2} - \frac{h^2}{6} \right) = \frac{G}{\eta} \left(\frac{h^3 R_c}{12} - \frac{h^4}{24} \right), \tag{5.2.18}$$

$$G = -\frac{6\eta}{R_c h^3} \left(\frac{q_p}{\pi} + v R_c h \left(1 - \frac{h}{3R_c} \right) \right) \left(1 - \frac{h}{2R_c} \right)^{-1}, \tag{5.2.19}$$

There will be a significant shear stress on the capillary wall. The shear stress at $y = 0$ is

$$\sigma_{yz} = \eta \frac{\partial v_p}{\partial y} = -\frac{\eta G h}{2\eta} + \frac{v}{h}\eta, \tag{5.2.20}$$

$$\sigma_{yz} = \frac{3\eta}{R_c h^2} \left(\frac{q_p}{\pi} + v R_c h \right) + \eta \frac{v}{h}, \tag{5.2.21}$$

$$\sigma_{yz} = \frac{3 q_p \eta}{R_c h^2 \pi} + \frac{4\eta v}{h}. \tag{5.2.22}$$

The total force on the cylindrical wall is

$$F_{c12} = 2\pi R_c \int_{z_1}^{z_2} \sigma_{yz} dz = 2\pi R_c \eta \int_{z_1}^{z_2} \left(\frac{3 q_p}{R_c h^2 \pi} + \frac{4v}{h} \right) dz. \tag{5.2.23}$$

With the known expression for h inserted, this becomes

$$F_{c12} = \frac{2\pi R_c \eta}{h_0} \int_{z_1}^{z_2} \left(\frac{3 q_p}{h_0 \pi R_c \left(1 + \frac{z^2}{d^2} \right)^2} + \frac{4v}{1 + \frac{z^2}{d^2}} \right) dz. \tag{5.2.24}$$

Bearing in mind that $R_p \ll d$, we achieve

$$F_{c12} = 8\pi\eta R_c v \frac{d}{h_0}\left(\pi - \frac{2d}{R_p}\right) + 6q_p \frac{\pi d}{2h_0^2}. \tag{5.2.25}$$

Next, the force balance between the particle surface (F_p) and the capillary wall (F_{c12}) yields

$$p_1 A_1 - p_2 A_2 - F_p - F_{c12} = 0, \tag{5.2.26}$$

where p_1 and p_2 are the fluid pressures at z_1 and z_2, and $A_1 = A_2$ are the cross-sectional areas between the particle and the capillary wall. By solving for $p_2 - p_1$ and inserting the known expression for G, we achieve

$$p_2 - p_1 = \int_{-R_p}^{R_p} G dz = -6\eta \int_{-R_p}^{R_p} \left(\frac{q_p}{\pi R_c}\left(\frac{1}{h^3} + \frac{1}{2R_c h^2}\right) + v\left(\frac{1}{h^2} + \frac{1}{6hR_c}\right)\right) dz. \tag{5.2.27}$$

We assume that the particle surface is force-free ($F_p = 0$). Consequently,

$$q_p = -\frac{4}{3}\pi R_c h_0 v \left(1 - \frac{5h_0}{3R_c} + \cdots\right). \tag{5.2.28}$$

The total pressure drop over the sphere is achieved by combining equations *(5.2.27)* and *(5.2.28)*:

$$\Delta p_{sp} = \frac{4\pi\eta d v}{h_0 R_c}. \tag{5.2.29}$$

Thus, the total pressure drop over the capillary tube containing a spherical particle is found by combining equations *(5.2.1)* and *(5.2.29)*:

$$\Delta p = \frac{8\eta v}{R_c^2}\left(L - 2R_p\right) + \frac{4\pi\eta d v}{h_0 R_c}. \tag{5.2.30}$$

Now, the equation for streaming potential exclusively due to the zeta potential on the capillary wall (I.e. $\zeta_p = 0, \zeta_c \neq 0$) is dealt with. This is essentially Helmholtz-Smoluchowski's equation for single phase streaming potential derived from Poiseuille's equation and Poisson's equation, here expressed by the pressure gradient G instead of the pressure difference Δp:

$$\frac{dE_c}{dz} = \frac{\varepsilon \zeta_c G}{\eta \lambda}, \tag{5.2.31}$$

where E_c is the streaming potential due to zeta potential on the capillary wall, and ζ_c and ζ_p are the zeta potentials on the capillary wall and on the spherical particle respectively.

When the spherical particle is present, the capillary fluid velocity is $v_c = v_p + v$, where the particle velocity is given by equation *(5.2.14)*. Considering the streaming current I_s is equal in magnitude and opposite direction of the conduction current I_c, we have

$$\frac{dE_c}{dz} = -\frac{2\pi R_c \varepsilon \zeta_c}{A\lambda}\left(\frac{4v}{h} + \frac{3q_p}{\pi R_c h^2}\right), \tag{5.2.32}$$

where A is the cross-sectional area available for flow, expressed as $A = \pi(R_c^2 - (R_c - h)^2) \approx 2\pi R_c h$ when $h \ll R_p$, and q_p is the flux through the gap. Thereby, the streaming potential over the sphere is obtained by integrating from $-R_p$ to R_p:

$$E_c = -\int_{-R_p}^{R_p} \frac{dE_c}{dz}\, dz = \frac{\varepsilon \zeta_c}{\lambda}\int_{-R_p}^{R_p}\left(\frac{4v}{h^2} + \frac{3q_p}{\pi R_c h^3}\right) dz, \tag{5.2.33}$$

$$E_c \approx \frac{\varepsilon \zeta_c d\pi v}{2\lambda h_0^2}. \tag{5.2.34}$$

Next, the streaming potential exclusively due to zeta potential on the spherical particle is considered (I.e. $\zeta_p \neq 0, \zeta_c = 0$). The procedure for the derivation will be similar as for streaming potential on the capillary wall, but the resulting equation has negative sign:

$$\frac{dE_p}{dz} = -\frac{\varepsilon \zeta_p G}{\eta \lambda}, \tag{5.2.35}$$

where E_p is the streaming potential due to zeta potential on the particle surface. By following the same procedure as above, we find that the streaming potential is

$$E_p \approx -\frac{\varepsilon \zeta_p d\pi v}{2\lambda h_0^2}. \tag{5.2.36}$$

Jackson (2008) showed that the correlation between single phase- and multi-phase streaming potentials are additive (i.e. $E_{s2} = E_c + E_p$). Thus, the total two-phase streaming potential for a single sphere becomes

$$E_{sp} = \frac{\varepsilon \zeta_c}{\lambda \eta}\Delta p + \frac{\varepsilon \pi v(\zeta_c - \zeta_p)d}{2\lambda h_0^2} + O\left(\frac{\varepsilon \pi v \zeta d}{\lambda h_0 R_c}\right), \tag{5.2.37}$$

where Δp is expressed by equation *(5.2.30)*, $O\left(\frac{h_0}{R_c}\right)$ is an order term and the two-phase streaming potential is referred to as E_{sp}. It can be shown that the order term is small by dividing it by the second term in the equation and treating ζ as equal to $(\zeta_c - \zeta_p)$, thereby

$$\frac{\varepsilon\pi v\zeta d}{\lambda h_0 R_c}\cdot\frac{2\lambda h_0^2}{\varepsilon\pi v(\zeta_c-\zeta_p)d}=\frac{h_0}{R_c}. \tag{5.2.38}$$

As long as the capillary radius R_c is much larger than the minimum gap width h_0, it is safe to neglect the order term. This leads to the simplified equation for the total streaming potential caused by a rigid spherical oil particle in a water-wet tube:

$$E_{sp}=\frac{\varepsilon\zeta_c\Delta p}{\lambda\eta}+\frac{\varepsilon\pi v(\zeta_c-\zeta_p)d}{2\lambda h_0^2}. \tag{5.2.39}$$

With the known expression for d inserted, this becomes

$$E_{sp}=\frac{\varepsilon\zeta_c\Delta p}{\lambda\eta}+\frac{\varepsilon\pi v}{2\lambda}(\zeta_c-\zeta_p)\sqrt{\frac{2R_p}{h^3}}. \tag{5.2.40}$$

It is customary normalise the two-phase streaming potential by the single-phase streaming potential in order to look at the deviation from the single-phase behaviour. The normalised equation becomes:

$$E_{sp,norm}=1+\frac{\pi\eta v}{2\zeta_c\Delta p}(\zeta_c-\zeta_p)\sqrt{\frac{2R_p}{h^3}}. \tag{5.2.41}$$

5.2.2. A Line of Non-Interacting Spherical Particles

Considering a capillary filled with a line of N spherical particles, sufficiently separated so that they do not interact, equation *(5.2.40)* can be further developed. The behaviour of the zeta potential at the capillary wall and on the particles is assumed the same as for the previous case. The number of particles is considered to be $N \ll L_c/R_c$. In this case, the expected total pressure drop (equation *(5.2.30)*) over the line of particles is expected to take the slightly different form:

$$\Delta p=\frac{8\eta v}{R_c^2}\left(L_c-2NR_p\right)+\frac{4N\pi\eta dv}{h_0R_c}, \tag{5.2.42}$$

accounting for the cumulative effect of all N particles. By following the same derivation procedure as in the previous section, the total two-phase streaming potential becomes

$$E_{line}=\frac{\varepsilon\zeta_c\Delta p}{\lambda\eta}+\frac{\varepsilon\Delta p(\zeta_c-\zeta_p)R_c^2d\pi}{8\lambda\eta h_0\left(2h_0\left(L_cN^{-1}-2R_p\right)+R_cd\pi\right)}+O\left(\frac{N\varepsilon\zeta d\pi v}{\lambda h_0R_c}\right). \tag{5.2.43}$$

Again, we can neglect the order term, which leads to the simpler form

$$E_{line} = \frac{\varepsilon\zeta_c\Delta p}{\lambda\eta} + \frac{\varepsilon\zeta_c\Delta p}{\lambda\eta} \cdot \frac{(\zeta_c - \zeta_p)R_c^2 d\pi}{8\zeta_c h_0\left(2h_0\left(L_c N^{-1} - 2R_p\right) + R_c d\pi\right)}. \tag{5.2.44}$$

Inserting for the known expression for d yields

$$E_{line} = \frac{\varepsilon\zeta_c\Delta p}{\lambda\eta} + \frac{\varepsilon\zeta_c\Delta p}{\lambda\eta} \cdot \frac{\pi R_c^2(\zeta_c - \zeta_p)\sqrt{2R_p h_0}}{8\zeta_c h_0\left(2h_0\left(L_c N^{-1} - 2R_p\right) + R_c\pi\sqrt{2R_p h_0}\right)}, \tag{5.2.45}$$

which can be normalised to

$$E_{line,norm} = 1 + \frac{\pi R_c^2(\zeta_c - \zeta_p)\sqrt{2R_p h_0}}{8\zeta_c h_0\left(2h_0\left(L_c N^{-1} - 2R_p\right) + R_c\pi\sqrt{2R_p h_0}\right)}. \tag{5.2.46}$$

Chapter 6. Analysis of the Two-Phase Models

In this chapter, numerical solutions of the models for two-phase streaming potential are computed and analysed using appropriate parameter values from experimental results at relevant conditions. The range of validity for the models are discussed and the effects on the streaming potential by the second phase are deliberated. This chapter presents the results subjected to further discussions in Chapter 7, where they are compared to recent experimental results for two-phase streaming potential.

6.1. Single Spherical Droplet Model

The effect of a single spherical droplet in a capillary can be expressed by equation *(5.2.41)*:

$$E_{sp,norm} = 1 + \frac{\pi\eta v}{2\zeta_c \Delta p}\left(\zeta_c - \zeta_p\right)\sqrt{\frac{2R_p}{h^3}}.$$

The two-phase streaming potential as described by this model depends on zeta potentials of the two interfaces and applied pressure difference, as well as conductivity, permittivity and viscosity of the formation water. All these parameters can be considered constant for a given rock/brine composition. The oil droplet is assumed fully insulating, possibly with a surface charge, and the capillary is water-wet. The streaming potential can thereby change as a function of particle radius and gap width between the particle and the capillary. Since the size of the oil particle directly indicates saturation, the possible relationship between two-phase streaming potential and water saturation must be examined.

In the derivation of the model first presented by Sherwood, it is assumed that lubrication theory can be applied. For this assumption to be valid, a few conditions must be met: The Debye length κ^{-1} is much smaller than the minimum gap width h_0, which again is much smaller than the radius of the particle R_p. There is only a slight difference between the particle radius and capillary radius. I.e.:

- $\kappa^{-1} \ll h_0$
- $h_0 \ll R_p, h_0 \ll R_c$

The minimum value of h_0 is only limited by maximum Debye length. The mathematical expression for the Debye length comes from the linearized Poisson-Boltzmann equation, where we have, from equation *(3.3.10)*:

$$\kappa^{-1} = \left(\sqrt{\frac{e^2}{\varepsilon k_B T} \sum_i n_i^0 \cdot z_i^2} \right)^{-1}.$$

For monovalent salts, this equation can be simplified to (Butt et al., 2006):

$$\kappa^{-1} = \left(\sqrt{\frac{2c_0 e^2}{\varepsilon k_B T}} \right)^{-1}, \tag{6.1.1}$$

where c_0 is the brine salinity in mol/L. If all factors are quantified for water at $400\ K$, the Debye length can be expressed as

$$\kappa^{-1} = \frac{3.41}{\sqrt{c_0}}\ x10^{-10}\ m. \tag{6.1.2}$$

For formation brine salinity of $200\,000\ ppm$ NaCl (McCartney & Rein, 2005), the corresponding Debye length is $\kappa^{-1} \approx 2x10^{-10}\ m$. For minimum salinity of $1000\ ppm$ NaCl used in low salinity water flooding (Austad, 2013), the corresponding Debye length is $\kappa^{-1} \approx 2x10^{-9}\ m$. Assuming *much less than* means at least one order of magnitude, this leads to $h_0 \geq 2x10^{-8}\ m$.

The minimum and maximum values for capillary radius is limited by realistic reservoir permeability. Permeability can be related to capillary radius by the *bundle of tubes* model. This model estimates the reservoir rock as a bundle of capillary tubes of radius R_c and length L. The pressure gradient acts over the length L_0 of the porous medium. The permeability can be expressed as:

$$k = \frac{nR_c^2}{8\tau^2}, \tag{6.1.3}$$

where n is the porosity and $\tau = \frac{L}{L_0}$ accounts for the tortuosity of the tubes. For the case with only one capillary tube, we have $\tau = 1$ and $n = 1$, which yields

$$k = \frac{R_c^2}{8}, \tag{6.1.4}$$

or

$$R_c = \sqrt{8k}. \tag{6.1.5}$$

Permeability of producible oil reservoirs on the NCS typically range from $100\ mD$ up to the order of $10\ D$. The capillary radius is thus limited by $R_{cmin} \approx 10^{-6}\ m$ and $R_{cmax} \approx 10^{-5}\ m$. At the same time, the particle radius must remain at least ten times greater than the minimum gap width.

The limiting values to ensure that the conditions for the derivation are met are summarized in Table 1:

Parameter	**Minimum Value**	**Maximum Value**	**Limited By**
κ^{-1}	$10^{-10}\ m$	$2x10^{-9}\ m$	Brine Salinity
h_0	$2x10^{-8}\ m$	$10^{-7}\ m$ (Low perm.) $10^{-6}\ m$ (High perm.)	Debye length, droplet size, capillary radius
R_c	$10^{-6}\ m$	$10^{-5}\ m$	Permeability
R_p/h_0	10	−	Lubrication theory

Table 1 Limiting values for lubrication theory.

In order to investigate a possible relationship between streaming potential and saturations for two-phase flow, we have to define the water saturation by the geometry of the sphere and the capillary. For one sphere in one capillary, the *local water saturation* can be defined as

$$S'_w = \frac{V_w}{V_c}, \tag{6.1.6}$$

where V_w is the volume of water and V_c is volume of the capillary. The local water saturation is defined as the saturation in the capillary volume limited by the capillary walls and $3R_c$ as illustrated in Figure 6.1. The capillary volume is thus $V_c = 3\pi R_c^3$. The droplet consists of oil and the surrounding phase is water. The local water saturation can further be expressed as

$$S'_w = \frac{V_c - V_o}{V_c} = \frac{3\pi R_c^3 - \frac{4}{3}\pi R_p^3}{3\pi R_c^3}, \tag{6.1.7}$$

$$S'_w(R_c, R_p) = \frac{R_c^3 - \frac{4}{9}R_p^3}{R_c^3}. \tag{6.1.8}$$

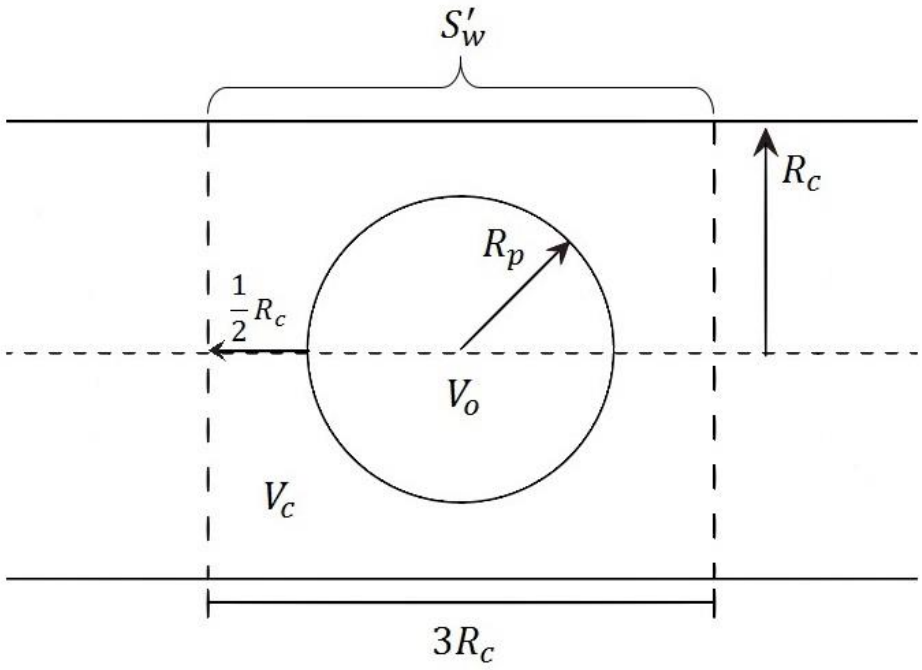

Figure 6.1 Definition of the local water saturation $S'_w(R_c, R_p)$. Lengths are not to scale.

To achieve an understanding of how the streaming potential varies with saturations, an example calculation of the model for spherical particle is carried out using typical values from experimental measurements performed by Vinogradov et al. (2010) and by Al-Mahrouqi (2016) in addition to Black et al. (2013).

Parameter	**Value**	**Comments**
ε_{LS}	$7x10^{-10}\ F/m$	LS: ~2000 $ppm \approx 0.04\ M\ NaCl$
ε_{HS}	$2.7x10^{-10}\ F/m$	HS: ~200 000 $ppm \approx 4\ M\ NaCl$
ζ_c	$-6x10^{-3}\ V$	
ζ_p	$-10x10^{-10}\ V$	
L_c	$0.07\ m$	
v	$10^{-3}\ m/s\ (12\ ml/min)$	For core dimensions $R = 1.9cm\ L = 7cm\ n = 0.18$
λ_{LS}	$0.5\ S/m$	LS: ~2000 $ppm \approx 0.04\ M\ NaCl$
λ_{HS}	$25\ S/m$	HS: ~200 000 $ppm \approx 4\ M\ NaCl$
η	$10^{-3}\ Pa \cdot s$	

Table 2 Values used for calculation of two-phase streaming potential (spherical model).

The electric potential at the interface between a sandstone and brine (ζ_c) is often negatively charged. Potentials at solid-brine interfaces for carbonates are often positive, but can be negative depending on pH and dissolved ions in the brine. A negative ζ_p at the oil-brine interface is common, and it is often more negative than the potential at the solid-brine interface (Al-Mahrouqi, 2016).

The results are plotted for different capillary radii to illustrate different values of permeability, where $R_c = 1\ \mu m$ corresponds to $k \approx 100\ mD$ and $R_c = 10\ \mu m$ corresponds to $k \approx 10\ D$. The first plot presented include the *local water saturation* as defined by equation *(6.1.8)* and Figure 6.1, where the lowest value of S'_w is limited by the minimum value of h_0 and the maximum value is limited by R_p/h_0.

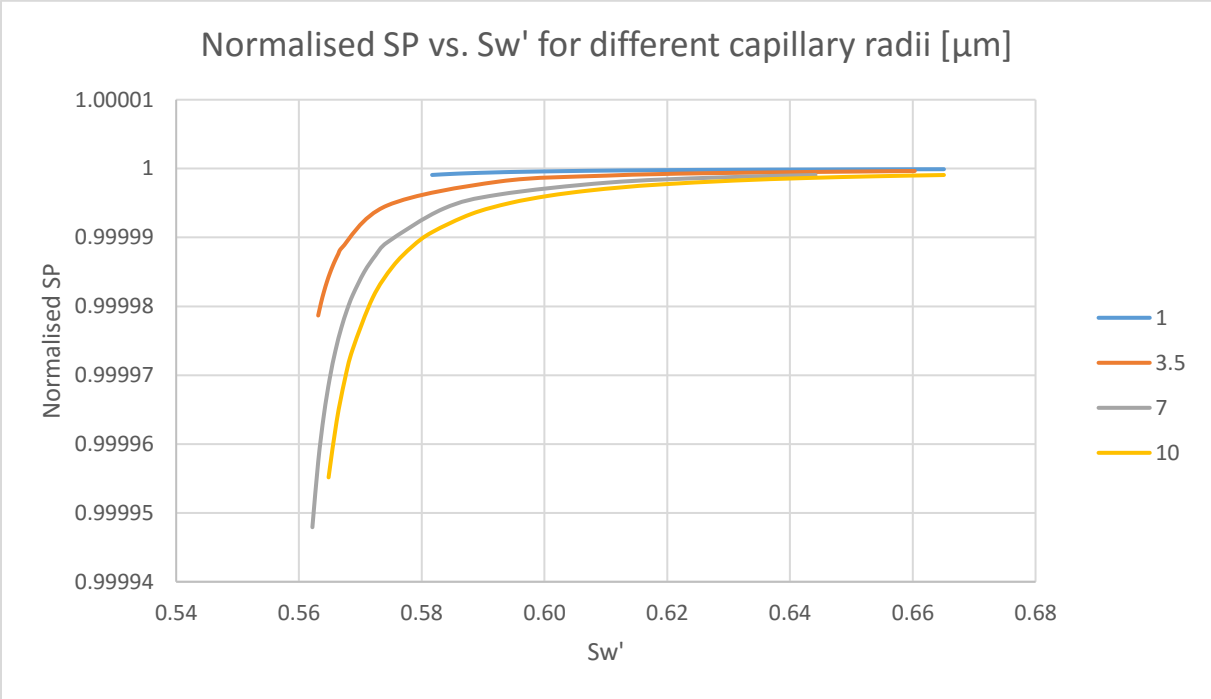

Figure 6.2 Normalised streaming potential vs. local water saturation for different capillary radii.

This plot shows two-phase streaming potential by the model for a single spherical particle in a circular capillary. The different lines represent different capillary sizes. The so-called local water saturation S'_w depends on the droplet- and capillary size. The normalised curves are equal for all salinities, since only permittivity and conductivity of the water phase changes (oil phase is assumed insulating). The effect of the oil phase generally seems to be largest for small capillaries, which could indicate a dependence on permeability. However, on closer inspection this effect appears because the local water saturation is not only a function of the particle radius, but also capillary radius and minimum gap width.

The oil saturation for a single particle could alternatively be expressed as the ratio between particle radius and capillary radius. Then, $1 - \frac{R_p}{R_c}$ can express some sort of water saturation. In this case, we see that the streaming potential is independent of capillary size (permeability). This agrees with the experimental results of Sprunt et al. (1994).

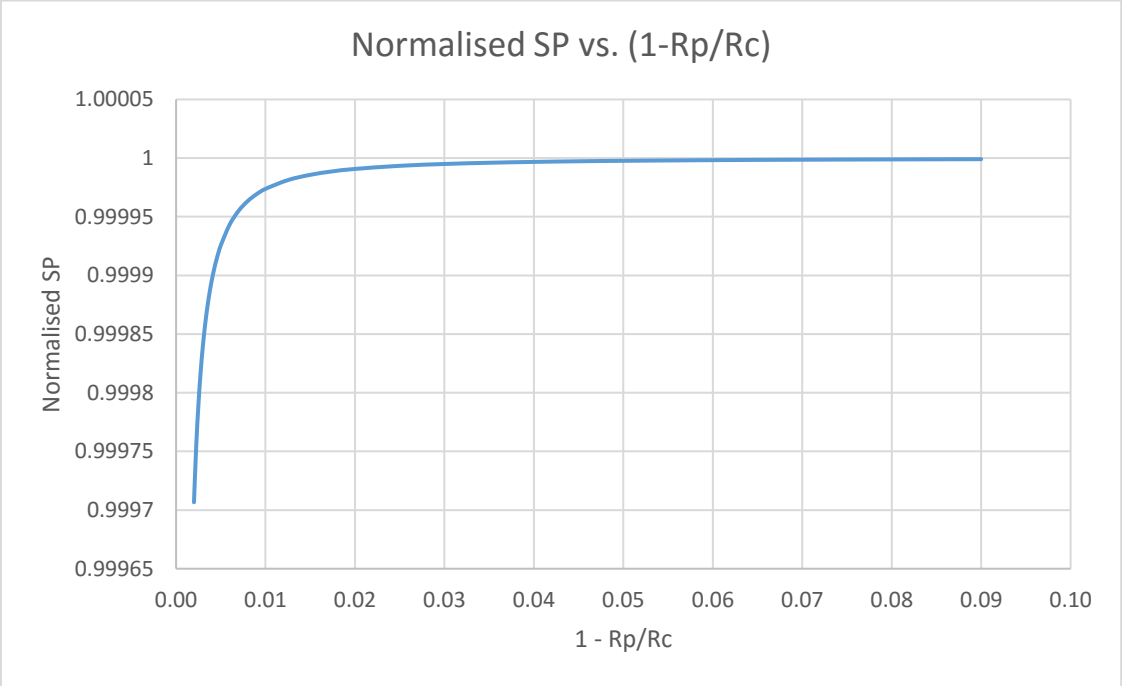

Figure 6.3 Normalised streaming potential vs. $(1 - R_p/R_c)$, where R_p/R_c represents the droplet size compared to capillary radius.

For the fluid velocity and zeta potential difference applied here, there appears to be essentially no change in streaming potential for a water-wet capillary partially filled with oil. Even for a higher difference between ζ_c and ζ_p, or for higher values of v, the change in streaming potential due to the non-wetting oil phase will be close to zero for realistic values of ζ_c, ζ_p and v. However, there is a clear trend in the plots even though the changes in streaming potential are small. As the oil droplet size increases, the streaming potential decreases. As the droplets become small, the effect of the second phase seems to disappear and the two-phase streaming potential approaches the single-phase streaming potential. It is likely that the model for a single particle in a capillary is too simple to capture the full effect of the oil phase. It is therefore necessary to perform a similar analysis of the model for a line of particles to see if the cumulative effect of many non-interacting particles creates a greater impact on the streaming potential.

6.2. A Line of Non-Interacting Spherical Particles

The change in streaming potential caused by a line of N non-interacting rigid spherical particles relative to single-phase is given by equation *(5.2.46)*:

$$E_{line,norm} = 1 + \frac{\pi R_c^2(\zeta_c - \zeta_p)\sqrt{2R_p h_0}}{8\zeta_c h_0\left(2h_0\left(L_c N^{-1} - 2R_p\right) + R_c\pi\sqrt{2R_p h_0}\right)}.$$

Similar to the model for a single spherical particle, the model for a line of particles also depends on zeta potential on the capillary wall and on the particle in addition to applied pressure difference and the properties of the formation water. Predictably, this model also depends on the number of particles in the capillary. In the derivation of this model, the number of particles is assumed to be $N \leq L_c/2R_c$ so that the total length of the line of particles is no longer than the length of the capillary. Based on laboratory measurements, this is a quantifiable size as we have the core plug length and capillary radius corresponding to permeability by the bundle of tubes model. We will investigate the relationship between the number of particles and the two-phase streaming potential, in addition to the effect of particle size. The factors limited by lubrication theory still apply and the same permeability (R_c) values are utilized. Thus to begin with, the values both from Table 1 and Table 2 are still valid.

To account for the line of particles, the definition of water saturation in the capillary must be redefined. The total fluid volume is now equal to the capillary volume

$$V_c = \pi R_c^2 L_c, \tag{6.2.1}$$

and the volume of the oil phase is the cumulative volume of all N particles

$$V_o = \frac{4}{3}\pi N R_p^3. \tag{6.2.2}$$

This gives the expression for the water saturation in the capillary as a function of the geometrics of a sphere within a circular tube and the number of particles:

$$S_w\left(R_c, R_p, L_c, N\right) = \frac{R_c^2 L_c - \frac{4}{3}N R_p^3}{R_c^2 L_c}. \tag{6.2.3}$$

To achieve and expression for the streaming potential as a function of water saturation, equation *(6.2.3)* can be solved for N

$$N = \frac{3R_c^2 L_c(1 - S_w)}{4R_p^3}, \tag{6.2.4}$$

and inserted into equation *(5.2.46)* to yield

$$E_{line}(S_w) = 1 + \frac{\pi R_c^2(\zeta_c - \zeta_p)\sqrt{2R_p h_0}}{8\zeta_c h_0\left(2h_0\left(\frac{4R_p^3}{3R_c^2(1-S_w)} - 2R_p\right) + R_c\pi\sqrt{2R_p h_0}\right)}. \tag{6.2.5}$$

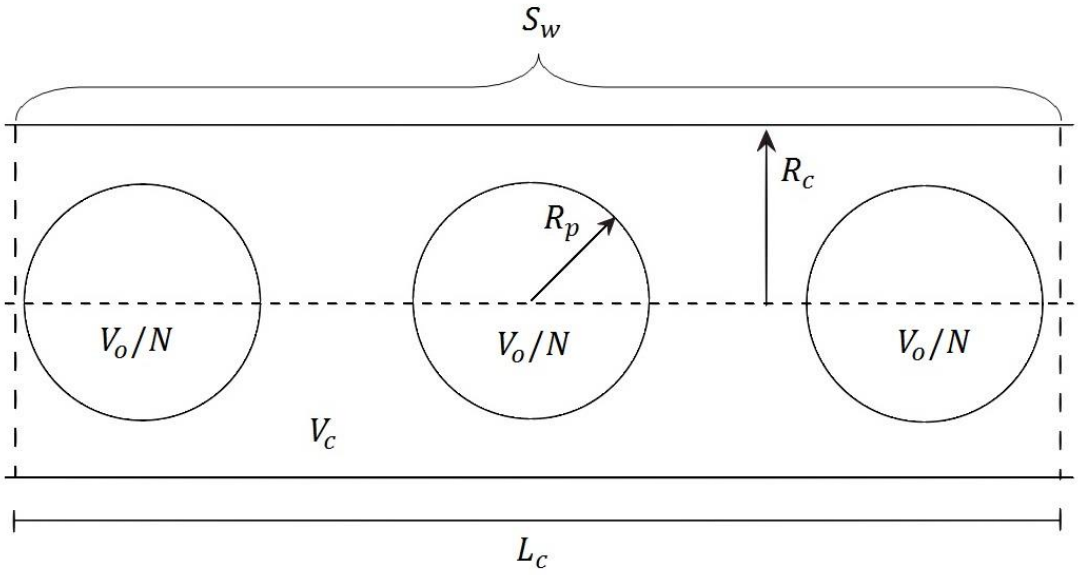

Figure 6.4 Definition of water saturation for a capillary filled with a line of spherical particles $S_w'(R_c, R_p, L_c, N)$.

Once again, a numerical computation is carried out to investigate the relationship between streaming potential and saturation in a water-wet capillary. The results are plotted for different particle sizes to investigate if this alters the streaming potential as for the single particle model. Figure 6.5 illustrates the reduction in streaming potential caused by a line of charged rigid particles in a capillary normalised by the single phase water saturation. The values used here can be found in Table 2. For decreasing water saturation, the streaming potential decreases towards zero. The model is limited by the maximum number of particles $N_{max} = \frac{L_c}{2R_p}$, which means that the model applies to water saturations above 0.5. It could seem like the SP-line would become negative for lower water saturations, but this will not happen for reasonable values of the zeta potentials as long as the limiting condition is met.

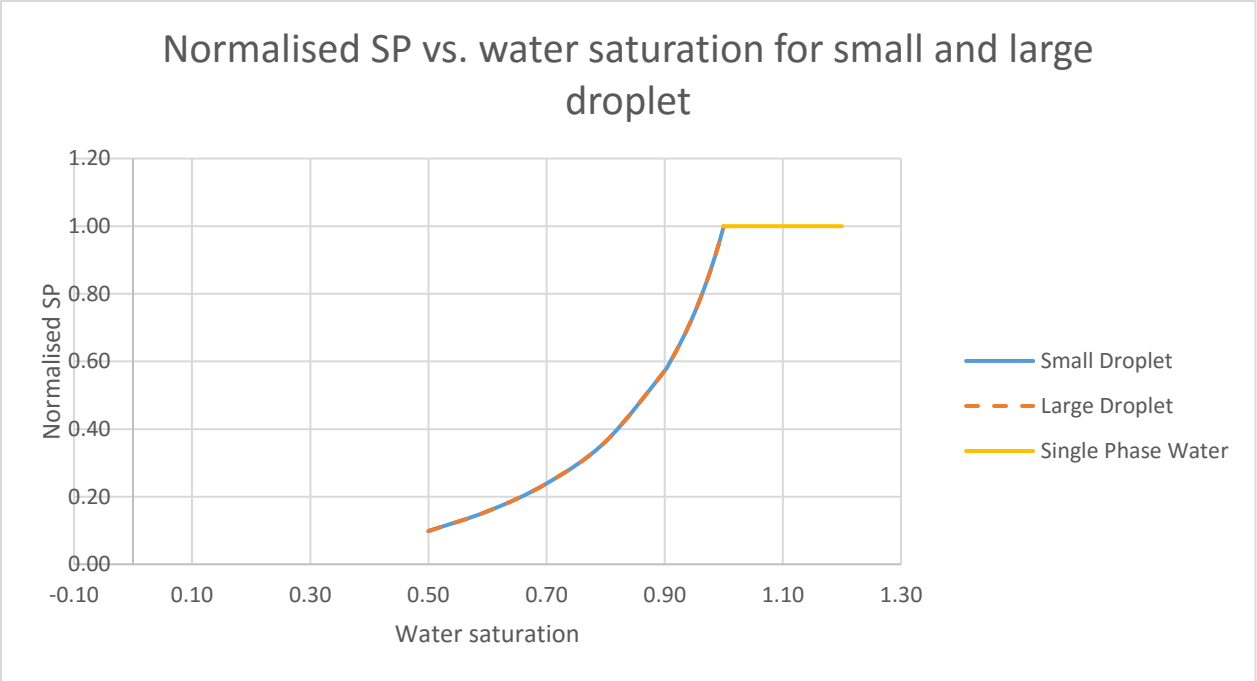

Figure 6.5 Normalised streaming potential vs. water saturation for small and large droplets. In addition, the single phase water line is indicated.

Here, *large droplet* refers to the largest droplet size in Figure 6.3 ($1 - \frac{R_p}{R_c} = 0.01$) and *small droplet* refers to the smallest ($1 - \frac{R_p}{R_c} = 0.09$). When a water saturation of 1 is reached, only the single phase streaming potential (Helmholtz-Smoluchowski) equation applies.

As expected, the accumulated effects of all N particles yields a significant change in streaming potential. For a water saturation of 50%, the non-wetting phase causes a reduction of the streaming potential by 90% compared to single phase water SP. This plot shows that the normalised two-phase streaming potential is effectively independent of droplet size, within the limitations of the model. The reason for this is not entirely clear. It could be that there is a very small effect of droplet size, but that the effect is dominated by the number of particles because that parameter is much larger.

To investigate the effects of different combinations of surface charge, a similar computation was completed for different electrokinetic potentials on the particle. The results are presented in Figure 6.6.

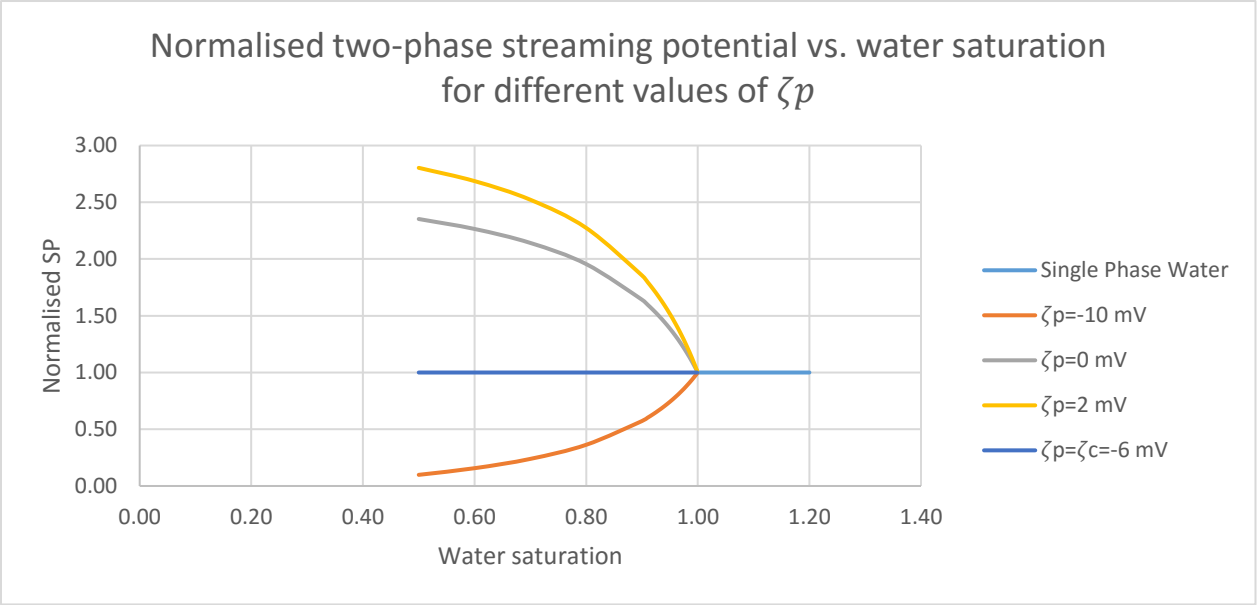

Figure 6.6 Normalised two-phase streaming potential vs. water saturation for different values of zeta potential on the particle (ζ_p).

Figure 6.6 shows the normalised streaming potential for different zeta potentials on the particles (ζ_p). The zeta potential on the capillary wall has a constant value of $\zeta_c = -6\ mV$. The contribution to the streaming potential from the rigid particles is negative for values of $\zeta_p < \zeta_c$ and positive for values of $\zeta_p > \zeta_c$. When $\zeta_p = \zeta_c$, the contribution from the particles is zero. This behaviour is expected and quite intuitive from the factor $(\zeta_c - \zeta_p)$ in equation *(5.2.46)*.

Chapter 7. Discussion

In this chapter, we discuss the results from Chapter 6 and some observations from other published material and experimental results. This is done in an effort to achieve a better understanding of how a second phase alters the measured streaming potential, and to characterize the importance of water saturation and wettability.

7.1. Results from Model Calculations and Experimental Data

The most apparent results from the computations in Chapter 6 is that the streaming potential can be highly affected by two-phase saturations, for a strongly water-wet system. It could be argued that the streaming potential is unaffected by the presence of an immobile droplet or particle. For an immobile droplet in a water-wet capillary, the water phase can move along the wall around the droplet as a response to an applied pressure difference. Thus, the streaming current, and consequently the streaming potential, can be developed without any influence from the droplet. Several experimental studies (e.g. (Al-Mahrouqi, 2016; Rahbar et al., 2017)) have claimed that the measurable change in streaming potential for two-phase flow is exclusively caused by alteration of wettability. The analysis and numerical computations of the simple models for two-phase streaming potential presented here indicate that the streaming potential may be affected by other processes in addition to wettability.

These models predict that the effect of oil saturation in a water-wet system can give a significant contribution to the total measured streaming potential. These contributions will be largest for particles/droplets with a zeta potential sufficiently different from the zeta potential on the capillary wall. It is possible that the model for a line of particles predicts reorganizing of the particles within the porous medium, not necessarily production of the oil phase. If this is the case, the model calculations do not necessarily contradict the previous experimental results, and the total effect on the electrokinetic coupling can be assigned to a combining effect of wettability alteration and reorganizing of charged particles.

7.2. The Effect of Particle (Drop) Boundary Condition

The results from the analysis of the two-phase models indicate that a particle with no surface charge can generate a large impact on the total streaming potential, as long as there is a difference in electrokinetic potential on the capillary wall and the particle surface. However, for an uncharged spherical particle, the results might be different. Sherwood's paper (2007) also includes an analysis of a spherical bubble with an uncharged, stress-free surface. The main difference between the cases of charged and uncharged surface is the fluid velocity boundary conditions. For the charged rigid particle presented in Chapter 5.2.1, we assumed no-slip boundary condition, which means that the velocity gradient close to the particle-brine interface is very large. However, for an uncharged bubble, the velocity gradient at the particle-fluid interface is assumed to be zero. It appears that the two different boundary conditions can have large effects.

The streaming potential equation for the uncharged bubble is developed in a similar way as for the rigid particle in Chapter 6, with different boundary conditions. The resulting equation for a single bubble becomes (Sherwood, 2007):

$$E_{bubble} = \frac{\varepsilon\zeta_c}{\lambda}\frac{2\pi v\sqrt{2R_p h_0}}{h_0 R_c}. \tag{7.2.1}$$

This is a factor of $\frac{4h_0}{R_c}$ smaller than the equivalent result for a charged rigid particle. The assumption that $h_0 \ll R_c$ indicates that the effect of an uncharged bubble may be as much as one thousand times smaller than the effect of a charged rigid particle (considering $h_{0min} \approx 2x10^{-8}\ m, R_{cmax} \approx 10^{-5}\ m$). Therefore, the effect of a line of uncharged bubbles will likely be very small compared to a line of charged particles. For a stress free bubble, we have the fact that $\frac{\mu\partial u_p}{\partial y} = 0$ at the bubble interface. Clearly, this gives a low velocity gradient close to the surface at the bubble and a low shear of the double layer close to the bubble surface. Consequently, the streaming potential contribution is much lower than for a rigid particle.

So, what is the correct boundary condition to use in a realistic situation? This clearly depends on the chemical conditions at the particle/bubble surface. The surface of a an oil bubble in water can contain hydrophilic polar head-groups and hydrophobic non-polar tails (see Figure 7.1) (e.g. Shah (2012)). The roughness created by the hydrophilic head-group will create a large fluid velocity gradient near the interface. This will *stretch* the ions in the EDL, which will increase the effect on the streaming potential. For an uncharged surface with no velocity

gradient near the interface, this *stretching* of the EDL will not occur to a similar degree, and the impact on the total streaming potential will consequently be much smaller. Therefore the analysis presented here indicates that mobilized oil in the pores may give an observable contribution to the streaming potential if the oil is charged (as most crude oil are), and a very low contribution if the oil is uncharged. This can be tested in experiments.

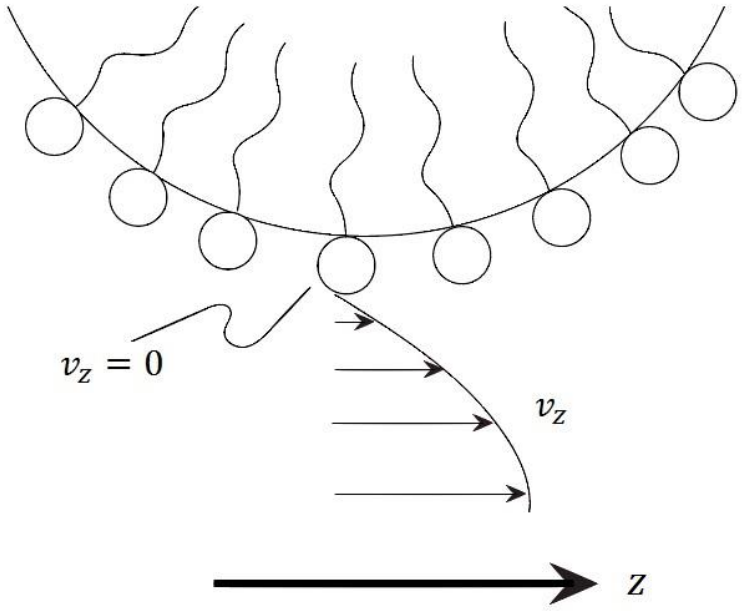

Figure 7.1 Illustration of the surface of a charged particle of oil dispersed in water with corresponding fluid velocity profile. The small spheres on the surface represent polar head-groups with a non-polar tail. The fluid moves in z-direction with velocity v_z. The polar head-groups decrease the fluid velocity to zero close to the particle surface.

Chapter 8. Conclusion

8.1. Concluding Remarks

The total streaming potential in a water-oil system is likely a combination of effects from wetting, movement of charged particles (drops) and movement of uncharged particles (drops). The total effect depends on the interface properties, and in particular, the electrokinetic potential and surface charge on the particles. The effect of saturation probably lies somewhere between the large effect of charged particles and the small effect of the uncharged particles. Depending on boundary conditions, this can affect the total streaming potential significantly.

8.2. Suggestions for Future Work

In order to explain the effects of two-phase streaming potential in further detail, we propose that effects of the boundary conditions for charged and uncharged particles be further examined. This is important to investigate, as these conditions appear to be very important for the effect of oil saturation on two-phase streaming potential. In this thesis we have not considered the effect of two phase streaming potential in more realistic networks of pores. To our knowledge this has not been done, and would be valuable to pursue. These models must (most likely) be solved numerically, and then it is extremely important how the boundary conditions at the surface of the bubble is implemented. In addition, it would be very interesting to investigate the behaviour of the streaming potential in micromodels, both with a non-polar and a polar oil.

References

Al-Mahrouqi, D. (2016). *Characterization of controlled salinity waterflooding in carbonate using streaming potential measurements.* Imperial College London.

Alkafeef, S. F., & Alajmi, A. F. (2006). Streaming potentials and conductivities of reservoir rock cores in aqueous and non-aqueous liquids. *Colloids and Surfaces A: Physicochemical and Engineering Aspects, 289*(1), 141-148.

Amott, E. (1959). Observations relating to the wettability of porous rock.

Appelo, C. A. J., & Wersin, P. (2007). Multicomponent diffusion modeling in clay systems with application to the diffusion of tritium, iodide, and sodium in opalinus clay. *Environmental science & technology, 41*(14), 5002-5007.

Atkins, P. W., & De Paula, J. (2010). Atkins' physical chemistry.

Austad, T. (2013). Water-based EOR in carbonates and sandstones: new chemical understanding of the EOR potential using smart water. *Enhanced oil recovery Field case studies*, 301-335.

Ban, H., Lin, B., & Song, Z. (2010). Effect of electrical double layer on electric conductivity and pressure drop in a pressure-driven microchannel flow. *Biomicrofluidics, 4*(1), 014104.

Bastow, T. P., van Aarssen, B. G., & Lang, D. (2007). Rapid small-scale separation of saturate, aromatic and polar components in petroleum. *Organic Geochemistry, 38*(8), 1235-1250.

Berg, J. (1993). *Wettability* (Vol. 49): Courier Corporation.

Black, M. J., Alhusseini, M., & Noui-Mehidi, M. N. (2013). High Salinity Permittivity Models for Water Cut Sensing. *IEEE Transactions on Instrumentation and Measurement, 62*(10), 2805-2811.

Briggs, D. R. (1928). The Determination of the Zeta Potential on Cellulose - A Method. *The Journal of Physical Chemistry, 32*(5), 641-675.

Butt, H.-J., Graf, K., & Kappl, M. (2006). *Physics and chemistry of interfaces*: John Wiley & Sons.

Campbell, N. A., & Reece, J. (2002). Biology, 5-th edition. *23*.

Carey, A., & Hayzen, A. (2001). The dielectric constant and oil analysis. *Practicing Oil Analysis Magazine, 9*.

Chandler, R. (1981). Transient streaming potential measurements on fluid-saturated porous structures: An experimental verification of Biot's slow wave in the quasi-static limit. *The Journal of the Acoustical Society of America, 70*(1), 116-121.

Chen, M., Raghuraman, B., Bryant, I., & Supp, M. (2006). *Streaming potential applications in oil fields.* Paper presented at the paper SPE 102106 presented at the 2006 Annual Technical Conference and Exhibition, San Antonio.

Delgado, Á. V., González-Caballero, F., Hunter, R., Koopal, L., & Lyklema, J. (2007). Measurement and interpretation of electrokinetic phenomena. *Journal of colloid and interface science, 309*(2), 194-224.

Dzyaloshinskii, I. E. e., Lifshitz, E., & Pitaevskii, L. P. (1961). General Theory of Van der Waals' Forces. *Physics-Uspekhi, 4*(2), 153-176.

Feynman, R. P., Leighton, R. B., & Sands, M. L. (1965). *The Feynman Lectures on Physics: Vol. 2: The Electromagnetic Field* (Vol. 2): Addison-Wesley.

Gustafsson, J., Mikkola, P., Jokinen, M., & Rosenholm, J. B. (2000). The influence of pH and NaCl on the zeta potential and rheology of anatase dispersions. *Colloids and Surfaces A: Physicochemical and Engineering Aspects, 175*(3), 349-359.
Hiemenz, P. C., & Rajagopalan, R. (1997). *Principles of colloid and surface chemistry*: CRC press.
Holman, J. (2002). Heat transfer, 9th: McGraw-Hill.
Hunter, R. J. (1981). *Zeta potential in colloid science: principles and applications* (Vol. 2): Academic press.
Israelachvili, J. N. (1985). Intermolecular and Surface Forces *Academic Press*.
Jackson, M. D. (2008). Characterization of multiphase electrokinetic coupling using a bundle of capillary tubes model. *Journal of Geophysical Research: Solid Earth, 113*(B4).
Jackson, M. D., & Vinogradov, J. (2012). Impact of wettability on laboratory measurements of streaming potential in carbonates. *Colloids and Surfaces A: Physicochemical and Engineering Aspects, 393*, 86-95.
Jackson, M. D., Vinogradov, J., Saunders, J. H., & Jaafar, M. Z. (2011). Laboratory measurements and numerical modeling of streaming potential for downhole monitoring in intelligent wells. *SPE Journal, 16*(03), 625-636.
Kendall, K. (1994). Adhesion: molecules and mechanics. *Science, 263*(5154), 1720-1726.
Lauga, E., Brenner, M., & Stone, H. (2007). Microfluidics: the no-slip boundary condition *Springer handbook of experimental fluid mechanics* (pp. 1219-1240): Springer.
Lin, K., Lu, C., Hsu, T., Chin, S., & Yen, A. (2012). Sub-20nm node photomask cleaning enhanced by controlling zeta potential. *Spie Newsroom*.
London, F. (1937). The general theory of molecular forces. *Transactions of the Faraday Society, 33*, 8b-26.
Malmberg, C., & Maryott, A. (1956). Dielectric Constant of Water from 0 to 100 C. *Journal of Research of the Natural Bureau of Standards, 56*.
McCartney, R., & Rein, E. (2005). *Formation waters of the Norwegian Continental Shelf.* Paper presented at the Tekna 16th International Oil Field Chemistry Symposium, Geilo, Norway.
Morrow, N. R. (1990). Wettability and its effect on oil recovery. *Journal of Petroleum Technology, 42*(12), 1,476-471,484.
Pascall, A. J., & Squires, T. M. (2011). Electrokinetics at liquid/liquid interfaces. *Journal of Fluid Mechanics, 684*, 163-191.
Rahbar, M., Jafarlou, A., Nejadali, M., Esmaeili, S., Pahlavanzadeh, H., & Ayatollahi, S. (2017). *Streaming Potential Measurement to Quantify Wetting State of Rocks for Water Based EOR, In-house Novel Setup Experience.* Paper presented at the IOR 2017-19th European Symposium on Improved Oil Recovery.
Revil, A., Schwaeger, H., Cathles, L., & Manhardt, P. (1999). Streaming potential in porous media: 2. Theory and application to geothermal systems. *Journal of Geophysical Research: Solid Earth, 104*(B9), 20033-20048.
Schindler, P., & Stumm, W. (1987). Aquatic surface chemistry. *Edited by W. Stumm*, 87.
Serway, R. A., Beichner, R. J., & Jewett, J. W. (2000). Physics for scientists and engineers with modern physics.
Shah, D. O. (2012). *Improved oil recovery by surfactant and polymer flooding*: Elsevier.
Shaw, D. J. (1980). Introduction to colloid and surface chemistry. 1992. *Butterworth-Heinemann, Oxford, ISBN 0, 7506*(1182), 0.
Sherwood, J. (2007). Streaming potential generated by two-phase flow in a capillary. *Physics of Fluids, 19*(5), 053101.
Spencer, N. D., & Moore, J. H. (2001). *Encyclopedia of chemical physics and physical chemistry: Applications* (Vol. 3): Taylor & Francis.

Sprunt, E. S., Mercer, T. B., & Djabbarah, N. F. (1994). Streaming potential from multiphase flow. *Geophysics, 59*(5), 707-711.
Stumm, W. (1992). *Chemistry of the solid-water interface: processes at the mineral-water and particle-water interface in natural systems*: John Wiley & Son Inc.
Tadmor, R. (2001). The London-van der Waals interaction energy between objects of various geometries. *Journal of Physics: Condensed Matter, 13*(9), L195.
Vinogradov, J., Jaafar, M., & Jackson, M. (2010). Measurement of streaming potential coupling coefficient in sandstones saturated with natural and artificial brines at high salinity. *Journal of Geophysical Research: Solid Earth, 115*(B12).
White, F. M., & Corfield, I. (2006). *Viscous fluid flow* (Vol. 3): McGraw-Hill New York.
Xie, Y., Sherwood, J. D., Shui, L., van den Berg, A., & Eijkel, J. C. (2011). Strong enhancement of streaming current power by application of two phase flow. *Lab on a Chip, 11*(23), 4006-4011.
Young, T. (1805). An essay on the cohesion of fluids. *Philosophical Transactions of the Royal Society of London, 95*, 65-87.
Ziauddin, M., Montaron, B., Hussain, H., Habashy, T., Seleznev, N., Signer, C., . . . Abdallah, W. (2007). Fundamentals of Wettability. *Schlumberger Oilfield Review*.

All figures are created by the author unless otherwise stated.